

043
RAW
13748

MOTION OF CHARGED PARTICLES IN PERIODIC
MAGNETIC FIELDS

by

SUNIL PAL SINGH RAWAT

A THESIS
SUBMITTED FOR THE DEGREE OF

DOCTOR OF PHILOSOPHY

OF THE
GUJARAT UNIVERSITY

AUGUST 1988

043

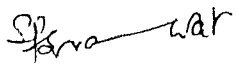


B13748

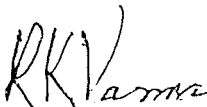
PHYSICAL RESEARCH LABORATORY
AHMEDABAD 380 009
INDIA

CERTIFICATE

I hereby declare that the work presented in this thesis is original and has not formed the basis of the award of any degree or diploma by any University or Institution.


Sunil Pal Singh Rawat
Author

Certified by:


R.K. Varma
(Professor-in-Charge)

Place : Ahmedabad

Date : 29-8-1988

CONTENTS

		<u>Page</u>
	Statement	1
	Acknowledgements	2
	List of Figures	3-10
CHAPTER I	Introduction	11-48
I.1	Quantum-like Theory for the Motion of Charged Particles in Inhomogeneous Magnetic Fields	15
I.2	Quantum-like Tunneling and Multiple Life Times	22
I.3	Bragg-like Reflections of Charged Particles in a Multimirror System	24
I.4	Survey of Theoretical, Numerical and Experimental Investigations of Motion of Charged Particles in Spatially Periodic Magnetic Field	29
I.5	Discussion	45
CHAPTER II	Experimental Arrangement	49-72
II.1	Vacuum System	50
II.2	Magnetic Field System	53

II.3	Electron Gun	61
II.4	Diagnostics	65
CHAPTER III	Experiments, Observations and Analysis	73-99
III.1	Dependence of Transmitted Electron Current on the Magnetic Field	74
III.2	Dependence of the Position of Dips on the Beam Energy	80
III.3	Dependence of the Position of Dips on the Injection Angle	82
III.4	Measurements Carried Out at Different Axial Positions	83
III.5	Energy Analysis at the Position of Dips and Peaks of the Transmitted Current Plot	91
CHAPTER IV	Discussion, Conclusions and Scope for Future Work	100-113
References		114-116

STATEMENT

The primary aim of the work described in this thesis is to study the motion of charged particles in spatially periodic magnetic fields as that of a multimirror system and to look for effects predicted by Schroedinger-like equations for the non-adiabatic behaviour of an ensemble of charged particles in inhomogenous magnetic fields.

The theory, wherein the Schroedinger-like equations have been obtained, some important predictions arising out of it along with a survey of other theoretical, numerical and experimental investigations of the motion of charged particles in a spatially periodic magnetic field are discussed in Chapter I.

The experimental device, designed and set up for verifying the occurrence of Bragg-like reflections is described in Chapter II.

Details of the experiments carried out with the abovementioned objective in mind are discussed in Chapter III. Consequent observations and analysis are also presented therein.

A summary with conclusions and scope for future work is presented in Chapter IV.

ACKNOWLEDGEMENTS

The work presented in this thesis was carried out under the supervision of Prof. R.K. Varma. I am grateful to him for his guidance.

I gratefully acknowledge the help and constant encouragement extended by Dr. A.M. Punithavelu without which it would have been difficult to complete the work.

The experimental work presented in this thesis was supplemented by the efficient technical assistance of R.C. Shah, Mrs. U. Modi, A.H. Shaikh and M.G. Phadke. The help rendered by M/s. M.P.K. Kurup and K.K. Sivasankaran from the glass blowing section and H.C. Patel from the workshop is appreciated.

I owe immensely to my friends and colleagues Shishir, Debashish, Vijayasanker, K.P. Subramanian, Jitesh, Vinod, N.N. Rao, S.C. Tripathi, Debi, Nikam, Bhaskaran, Subrat and B.P. Pande for their cooperation and help during the course of the work in some way or the other.

I sincerely thank Mr. V.T. Viswanathan for neat and efficient typing of the thesis. My thanks are also due to M/s. H.S. Panchal, S.C. Bhavsar for drafting and D.R. Ranpura for photography. I also thank Mrs. R.R. Bharucha, Mrs. Ghiya, Mrs. Patil and other library staff for their cooperation.

LIST OF FIGURES

	<u>Page</u>
Fig. 1.1 (a) Magnetic mirror field configuration	14
1.1 (b) Schematic representation of the adiabatic potential as a function of the co-ordinate X along a field line of the mirror configuration.	14
1.1 (c) Schematic representation of the loss cone in the velocity space configuration.	14
Fig. 1.2 (a) Dependence of the life times on the magnetic field for two different shapes of the field at mirror throat.	25
1.2 (b) Three life times as a function of the maximum magnetic field.	25
Fig. 1.3 (a) The analyzer current as a function of retarding potential at an anode voltage $V_0 = 2$ kV and a magnetic field	33

$H_0 = 136$ oerst. for various values of the modulating field h .

1.3 (b) The transverse energy as a function of magnitude of the modulating magnetic field h with $V_0 = 2$ kV and $H_0 = 136$ oerst. 33

1.3 (c) The transverse energy as a function of the number of periods n , traversed by the electron with $V_0 = 2$ kV and $H_0 = 136$ oerst. 33

Fig. 1.4 ξ as a function of ψ for values of a, b n upto 10 and $h = 0.05$ and 0.025 respectively. 37

Fig. 1.5 Radial ion motion, energy transfer coefficient and axial derivative of the transverse energy, $d\psi_1/dz$, in a multiple mirror with cell length $L_c = 10$ cm, cell number $N = 6$, mirror ratio $R_m = 1.3$. At the ion injection point $z = 0$, the radial position of the ion is $r_0 = 1.0$ cm. Initial beam energy is (a) $\psi_b = \psi_{bR}$ 42

($V_b = f_c L_c$) and (b) $\Psi_b = 1.25 \Psi_{bR}$.

Fig. 1.6 (a) Axial ion current $I_{c||}$ at the entrance position near the axis (13 cm upstream from the first mirror point).

44

(b) Axial ion current $I_{c||}$ at an exit position of the multiple mirror near the axis (10 cm downstream from the last mirror point).

44

(c) $I_{c\perp}$ at the same position of (b) as a function of the injected beam energy Ψ_b . B_0 is fixed at 2.7 KGauss.

44

Fig. 1.7 Variations of

46

(a) axial energy distribution
(b) transverse energy distribution
near the axis at the exit position of the multiple mirror as function of the injected beam energy.

$\Psi_b = 23$ eV corresponds to the resonance condition.

		6
Fig. 2.1	Multimirror machine	51
Fig. 2.2	Schematic of the experimental device	52
Fig. 2.3	Block diagram of Electropneumatically controlled vacuum system	54
Fig. 2.4	Block diagram of power connections to magnetic field coils	57
Fig. 2.5	Computer plots of magnetic field distribution	59
Fig. 2.6	Experimental plots of magnetic field distribution	60
Fig. 2.7	Schematic of the electron gun	63
Fig. 2.8	I-V characteristic and energy spectrum of electron beam	64
Fig. 2.9	Electron gun with mechanism for varying injection angle and radial position	66
Fig. 2.10	Retarding potential analyzer mounted on the trolley	68

- Fig. 2.11 Block diagram for obtaining
transmitted electron current
versus magnetic field plot 70
- Fig. 2.12 Block diagram for obtaining I-V
characteristic with the retard-
ing potential analyzer 71
- Fig. 3.1 Transmitted electron current as
a function of magnetic field,
recorded 10 mirrors away from
the electron gun, beam energy =
800 eV, injection angle = 32° . 76
- Fig. 3.2 Transmitted electron current
versus magnetic field plots
recorded 13 mirrors away from
the gun at different analyser
grid voltages. Beam energy =
1000 eV, injection angle =
 32° and mirror ratio = 1.06. 78
- Fig. 3.3 Dependence of the position of
the dips in transmitted current
on square root of electron beam 81

energy in the third mirror region. Mirror ratio = 1.06.

- Fig. 3.4 Dependence of the position of the dips in transmitted current on injection angle θ in the third mirror region. Mirror ratio = 1.06. 84
- Fig. 3.5 Transmitted electron current as a function of magnetic field at different axial positions. Beam energy = 800 eV, injection angle = 37° and mirror ratio = 1.06. 85, 86, 87
- Fig. 3.6 Position of dips as a function of distance from the electron gun. Beam energy = 800 eV, injection angle = 37° and mirror ratio = 1.06. 90
- Fig. 3.7 Spectrum of parallel energy of electrons at the first dip at different distances from the gun. Beam energy = 600 eV, injection angle = 37° and mirror ratio = 1.06. 92

- Fig. 3.8 Parallel energy of electrons at the first dip as a function of distance from the electron gun. Beam energy = 600 eV, injection angle = 37° and mirror ratio = 1.06. 93
- Fig. 3.9 Spectrum of parallel energy at different magnetic fields. Beam energy = 600 eV, injection angle = 37° and mirror ratio = 1.06. 95, 96
- Fig. 3.10 Peak of parallel energy as a function of magnetic field. Beam energy = 600 eV, injection angle = 37° and mirror ratio = 1.06. 97
- Fig. 3.11 Transmitted electron current versus magnetic field, recorded 10 mirrors away from the electron gun, showing various orders and modes of the relation $\ell \Omega = n \omega_t$. Beam energy = 600 eV, inje- 98

ction angle = 37° and

mirror ratio = 1.06.

Fig. 4.1 Observable modes and orders at various
distances from the electron gun

107

CHAPTER I

Introduction

The study of motion of charged particles in inhomogeneous magnetic fields such as that of a magnetic mirror is important from the point of view of its various applications to laboratory as well as space and astrophysical plasmas like mirror plasmas and Van Allen radiation belts. Since the equations of motion in such fields are highly nonlinear, it is in general, not possible to solve for the motion analytically; only numerical solutions can be obtained by using a computer. One has, therefore, to invoke approximations. Guiding centre approximation is one such approximation, which results when the fields vary slowly, that is, the fractional change of magnetic field over a gyroradius or gyroperiod is very small compared to unity i.e.,

$$\frac{\lambda_L}{B} \nabla B \ll 1 \quad \text{or} \quad \frac{\lambda_L}{L} \ll 1 \quad (1.1)$$

and
$$\frac{1}{\Omega B} \frac{\partial B}{\partial t} \ll 1 \quad (1.2)$$

where $\Omega = eB/m$ is the cyclotron frequency; $r_L = v_\perp / \Omega$ is the Larmor radius; v_\perp being the perpendicular component of the velocity of the particle and L , the scale length of the inhomogeneity of magnetic field. In this approximation the adiabatic action $\mu = 1/2 m v_\perp^2 / \Omega$ is invariant. As a consequence of the invariance of μ , the motion along the field line reduces to a motion in an effective potential $V = \mu \Omega$. The adiabatic equation of motion is given by¹

$$m \frac{dv_\parallel}{dt} = -\nabla_\parallel (\mu \Omega) \quad (1.3)$$

Since the adiabatic potential $\mu \Omega$ is proportional to the strength of the magnetic field, this equation of motion offers the possibility of trapping charged particles in an adiabatic potential well, that is, in a region of weaker magnetic field bounded on either side by regions of stronger magnetic field, provided the energy E of the particles is less than the height of the potential $\mu \Omega_{\max}$

$$E < \mu \Omega_{\max} \quad \Omega_{\max} = \frac{e B_{\max}}{m} \quad (1.4)$$

Such a scheme for trapping of charged particles is the basis for one of the primary schemes for plasma confinement, the magnetic mirror trap² (Fig. 1.1a,b).

If θ_0 denotes the pitch angle of the particle in the mid plane of the mirror trap, where the magnetic field is B_0 , so that $V_{\perp} = V \sin \theta_0$ and $E_{\perp} = E \sin^2 \theta_0$, then for trapping

$$\sin^2 \theta_0 > \frac{B_0}{B_{\max}} \quad (1.5)$$

The ratio, B_{\max}/B_0 is an important parameter for magnetic mirror trap and is called 'mirror ratio', R_M . All such particles, which satisfy $E < \mu \Omega_{\max}$ or $\sin^2 \theta_0 > B_0/B_{\max}$, are trapped adiabatically. Conversely, particles which do not satisfy these inequalities will not be present in the trap. Smallest θ_0 , (θ_m), of a trapped particle is given by³

$$\sin^2 \theta_m = \frac{B_0}{B_{\max}} = \frac{1}{R_M} \quad (1.6)$$

This equation defines the boundary of a region in velocity space in the shape of a cone, called a loss cone (Fig. 1.1c). As the particles with velocity vectors inside the loss cone do not exist in the trap, trapping is never isotropic in a mirror.

If the invariance of μ were exact, the trapping of the charged particles would be perpetual. Since, as we have noted earlier, the invariance is only approximate, any departure from it would lead to particle losses from the adiabatic potential well. This phenomenon of escape of charged particles has been observed in many experiments^{4,5} and has been the subject matter of investigation by many authors using different approaches^{6,7}.

In the first section of this chapter we have reproduced

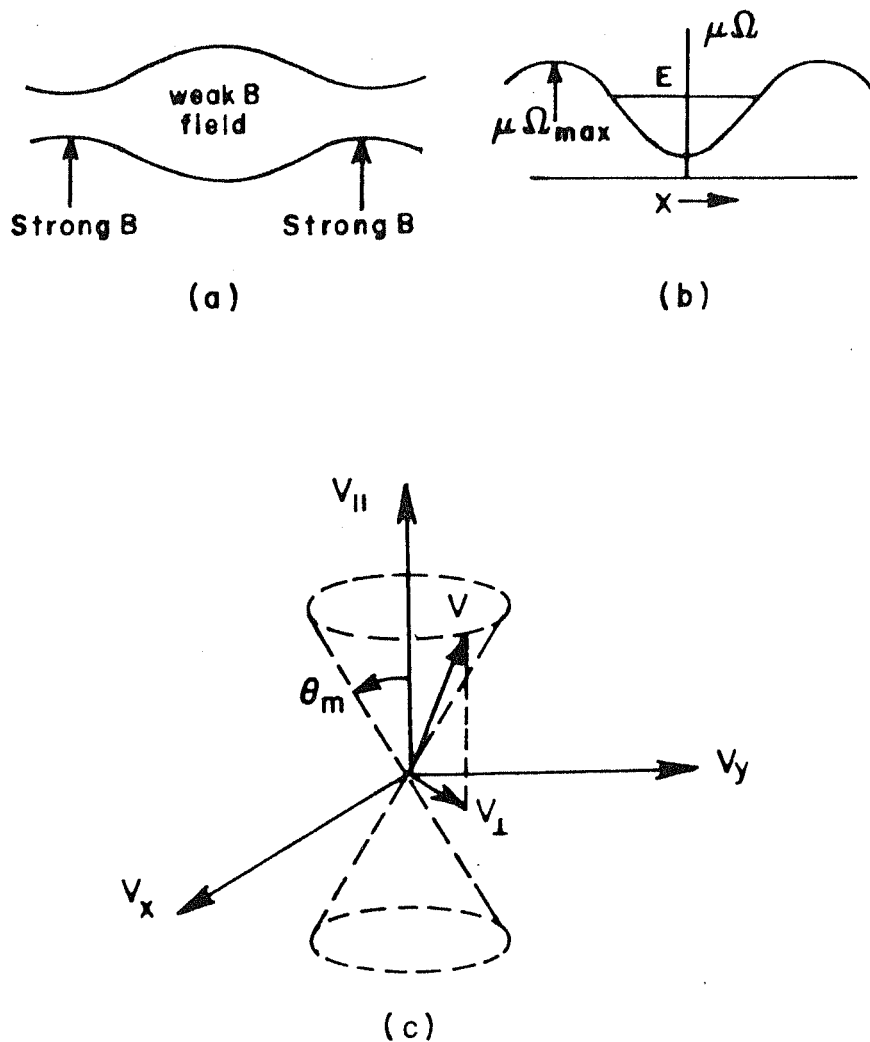


Fig. 1.1 (a) Magnetic mirror field configuration
 (b) Schematic representation of the adiabatic potential as a function of the co-ordinate x along a field line of the mirror configuration.
 (c) Schematic representation of the loss cone in the velocity space configuration.

in detail the quantum like theory proposed by R.K. Varma^{8,9} for the non-adiabatic behaviour of charged particles in inhomogeneous magnetic fields. In this formulation the non-adiabatic escape of particles from the adiabatic potential well turns out to be in the nature of tunnelling in quantum mechanics. This detailed description is necessitated by the fact that, as we shall see further in section (1.3), this theory predicts certain important consequences, the experimental verification of which has been the subject matter of the present work.

1.1. Quantumlike Theory for the Motion of Charged Particles in Inhomogeneous Magnetic Fields

As mentioned earlier, the motion of charged particles in inhomogeneous magnetic fields is nonlinear. Initial conditions in such a motion are very important. Evolution of particles' motion with different initial conditions will be in general different. Adiabatic approximation which provides the description of motion without taking the initial conditions like different Larmor phases of the particles into consideration, is thus incapable of describing the true motion.

In the approach adopted by Varma⁹, the behaviour of this motion is described through an ensemble viewpoint. As the projections of ensemble of exact motion on parallel magnetic field lines are considered to be very close to adiabatic motion, the non-adiabatic behaviour turns out to be a statistical property of the neighbourhood of the

adiabatic motion.

An ensemble of charged particles with a given energy E_0 and action μ is considered. The particles have a distribution in Larmor phase angle ϕ_0 . These particles are injected into an axisymmetric magnetic mirror trap.

The motion of particles in a magnetic field is described by the Lagrangian

$$L = \frac{1}{2} m (\dot{x}_{\parallel}^2 + \dot{x}_{\perp}^2 + \Lambda^2 \dot{\theta}^2) + \frac{e}{c} \Lambda \dot{\theta} A_{\theta} \quad (1.7)$$

Equivalent description of motion is given by the Hamiltonian

$$\bar{H} = \frac{p_{\parallel}^2}{2m} + \frac{p_{\perp}^2}{2m} + \frac{1}{2m\Lambda^2} \left[M - \frac{e}{c} \Lambda A_{\theta} \right]^2 \quad (1.8)$$

where x_{\parallel} and x_{\perp} are the co-ordinates along and perpendicular to the magnetic field lines, p_{\parallel} and p_{\perp} are the corresponding momenta, A_{θ} is vector potential and M is the canonical angular momentum given by

$$M = P_{\theta} = \frac{\partial L}{\partial \dot{\theta}} = m\Lambda^2 \dot{\theta} + \frac{e}{c} \Lambda A_{\theta} \quad (1.9)$$

From the Liouville equation, equations for the description of the exact (non-adiabatic) behaviour of the ensemble of charged particles are obtained. Liouville equation for the evolution of density of the ensemble of particles in phase space of canonical variables $(x_{\parallel}, p_{\parallel}, x_{\perp}, p_{\perp})$ is given by

$$\frac{\partial f}{\partial t} + \frac{p_{||}}{m} \frac{\partial f}{\partial x_{||}} + \frac{p_{\perp}}{m} \frac{\partial f}{\partial x_{\perp}} + p_{||} \frac{\partial f}{\partial p_{||}} + p_{\perp} \frac{\partial f}{\partial p_{\perp}} = 0 \quad (1.10)$$

This equation expresses the conservation of probability, along exact trajectories.

The initial distribution function f_0 is taken to be a δ -function in energy E , the canonical angular momentum P_{θ} and in action μ . The distribution $g(\phi_0)$ in the initial phase ϕ_0 is, however not controllable in an experiment.

Hamilton-Jacobi equation for this system can be written as

$$\frac{\partial S}{\partial t} + \bar{H} \left[\frac{\partial S}{\partial x_{||}}, \frac{\partial S}{\partial x_{\perp}}, x_{||}, x_{\perp}, t \right] = 0 \quad (1.11)$$

where $S = S(x_{||}, x_{\perp}, t)$ is the Hamilton's principal function and Hamiltonian

$$\bar{H} = \frac{1}{2m} \left[\frac{\partial S}{\partial x_{||}} \right]^2 + \frac{1}{2m} \left[\frac{\partial S}{\partial x_{\perp}} \right]^2 + \frac{1}{2m\lambda^2} \left[m - \frac{e}{c} \lambda A_{\theta} \right]^2 \quad (1.12)$$

Let S be a complete solution of the Hamilton-Jacobi equation. It is a function of constants of motion α_i , which are the momenta. So

$$S = S(x_{||}, x_{\perp}, t; \alpha_i) \quad (1.13)$$

For the initial values of the canonical co-ordinates β_i , following relation is given

$$\beta_i = \frac{\partial S}{\partial \alpha_i} \quad (1.14)$$

Any arbitrary function $f(\alpha_i, \beta_i)$ of the constants of motion α_i and β_i is a solution of the Liouville equation. For α_i energy E , canonical angular momentum P_θ and the initial value of the action μ were chosen with δ -function distribution in each of them.

β_i is transformed to $(x_{||}, \phi)$ resulting in a mixed representation of variables $(x_{||}, \phi, t; \alpha_i)$. The distribution function $f(x_{||}, \phi, t; \alpha_i)$ is the probability of finding a particle at $(x_{||}, \phi)$ at time t , if particle has initial momenta α_i (E, P_θ and μ). ϕ is the Larmor phase at time t defined by $\phi = \phi_0 - \int_0^t \Omega d\tau'$

The initial value of μ has a δ -function distribution. Hence,

$$f(x_{||}, \phi, t; \alpha_i) = \hat{f}(x_{||}, \phi, t; \alpha_i', \bar{\mu}) \delta(\mu_0 - \bar{\mu}) \quad (1.15)$$

Liouville equation for the evolution of f is given by

$$\frac{\partial \hat{f}}{\partial t} + v_{||} \frac{\partial \hat{f}}{\partial x_{||}} + \dot{\phi} \frac{\partial \hat{f}}{\partial \phi} = 0 \quad (1.16)$$

where $v_{||}$ and $\dot{\phi}$ are functions of $(x_{||}, \phi; \alpha_i)$. Liouville equation contains all the information about the evolution of the ensemble of charged particles. Exact details of trajectories are not necessary, and the description of non-adiabatic motion is sought in the neighbourhood of adiabatic motion through a variable $\Phi = (\phi + 1/\mu \int_0^t dt (1/2 m v_{||}^2))$, which is a functional variable and defines the neighbourhood of adiabatic motion through

the stationarity of Φ .

Liouville equation in terms of variable Φ can be written as

$$\frac{\partial f}{\partial t} + v \frac{\partial f}{\partial x} + \frac{L}{\mu} \frac{\partial f}{\partial \Phi} = 0 \quad (1.17)$$

where subscripts are dropped. Since f is the probability of finding a particle at (x, Φ) at time t , it has to be positive definite at all space-time point or

$$f = \Psi^2 \quad (1.18)$$

where Ψ is real.

A finite time integral form of f is given by

$$f(x, \Phi, t; \alpha_i') = f \left[x - \int_{t'}^t dt'' v, \Phi - \int_{t'}^t dt'' L/\mu, t'; \alpha_i' \right] \quad (1.19)$$

Also, using (1.18) and taking the square root

$$\Psi(x, \Phi, t; \alpha_i') = \Psi \left[x - \int_{t'}^t dt'' v, \Phi - \int_{t'}^t dt'' L/\mu, t'; \alpha_i' \right] \quad (1.20)$$

If Ψ is to be single valued, it must be periodic in larmor phase ϕ and also in Φ . Fourier series expansion of Ψ with respect of Φ is written as

$$\Psi(x, \Phi, t) = \sum_q \hat{\Psi}(x, q, t) e^{iq\Phi} \quad (1.21)$$

Fourier transform with respect to Φ gives

$$\hat{\Psi}(x, q, t) = \exp\left[-iq \int_t^t dt'' L/\mu\right] \hat{\Psi}\left[x - \int_{t'}^t v dt'', q, t'\right] \quad (1.22)$$

where $\int_{t'}^t L dt''$ is evaluated along the projections of the exact three-dimensional trajectories on the one-dimensional co-ordinate parallel to the magnetic field line. $\hat{\Psi}(x', q, t')$ at the space-time point (x', t') is propagated to a space-time point (x, t) connected by the trajectory $x = x' + \int_{t'}^t v dt''$. The propagator $\exp(-iq \int_{t'}^t L dt''/\mu)$ is a functional of trajectory.

Fourier transform of $\hat{\Psi}(x, q, t)$ with respect to x , (position at time t) is given by

$$\tilde{\Psi}(k, q, t) = \int \exp[+ikx] \hat{\Psi}(x, q, t) dx \quad (1.23)$$

or

$$\tilde{\Psi}(k, q, t) = \exp\left[+i \int_{t'}^t dt'' \left[qL/\mu - Kv\right]\right] \tilde{\Psi}(k, q, t') \quad (1.24)$$

A function $\bar{\Psi}$ is defined as

$$\bar{\Psi}(k, q, t) = \tilde{\Psi}^*(k, q, t) \exp\left[-\frac{1}{2} \frac{iqm}{\mu} \int_{t'}^t dt \left[v - \frac{\mu k}{mq}\right]^2\right] \quad (1.25)$$

In terms of $\bar{\Psi}$, Eq. (1.24) transforms to

$$\bar{\Psi}(k, q, t) = \exp\left\{-iq/\mu \int_{t'}^t dt'' \left[\frac{1}{2m} \left(\frac{\mu k}{q}\right)^2 + \mu \Omega\right]\right\} \bar{\Psi}(k, q, t') \quad (1.26)$$

Inverse Fourier transform of (1.26) with respect to k is given by

$$\psi(x, q, t) = \exp \left\{ -\frac{i q}{\mu} \int_{t'}^t dt'' \left[-\left(\frac{\mu}{q}\right)^2 \frac{1}{2m} \frac{\partial^2}{\partial x^2} + \mu \Omega[x(t'')] \right] \right\} \\ \times \psi(x, q, t')$$
(1.27)

Expansion of both sides around $t = t' + \tau$, with τ as an infinitesimal time gives

$$\left[1 + \tau \frac{\partial}{\partial t} + \frac{\tau^2}{2} \frac{\partial^2}{\partial t^2} + \dots \right] \psi(x, q, t') \\ = \left\{ 1 + \left[-\frac{i q}{\mu} \left[\int_{t'}^{t'+\tau} dt'' \left(-\frac{\mu^2}{q^2} \frac{1}{2m} \frac{\partial^2}{\partial x^2} \right) + \int_{t'}^{t'+\tau} \mu \Omega(x(t'')) dt'' \right] \right. \right. \\ \left. \left. + \dots \right\} \psi(x, q, t')$$
(1.28)

In the limit $\tau \rightarrow 0$

$$\int_{t'}^{t'+\tau} dt'' \Omega(x(t'')) = \Omega(x) \tau$$
(1.29)

and the following differential equation is obtained

$$i \frac{\mu}{q} \frac{\partial \psi}{\partial t} = -\left(\frac{\mu}{q}\right)^2 \frac{1}{2m} \frac{\partial^2 \psi}{\partial x^2} + (\mu \Omega) \psi$$
(1.30)

The total probability density $G(x, t)$ is then shown to be related to $\psi(x, q, t)$ in following way

$$G(x, t; \alpha_i') = \sum_q \psi^*(x, q, t; \alpha_i') \psi(x, q, t; \alpha_i')$$
(1.31)

This shows that the total probability density $G(x, t; \alpha_i')$ is

a sum of $\Psi^*(x, q, t; \alpha'_i) \Psi(x, q, t; \alpha'_i)$ over all the modes $q=1, 2, \dots$. In these equations (μ/q) appears in the role of \hbar and the adiabatic potential $\mu\Omega$ appears in place of the potential in the Schroedinger equation in quantum mechanics. The non-adiabatic effects thus appear in the nature of quantum effects in this formulation.

1.2. Quantum-like Tunnelling and Multiple Lifetimes

The above Schroedinger-like equations (1.30) predict quantum-like effects for the non-adiabatic ensemble behaviour of particles. In particular, these equations describe the quantum-like tunnelling of particles, having energy less than the maximum height of the adiabatic potential. This is identified with the non-adiabatic decay of particles from magnetic-mirror traps.

Life-times of particles of energy E and action μ , injected in a magnetic mirror trap may be calculated using the standard techniques of quantum mechanics. Different modes of the decay are predicted by the different equations of the set corresponding to $q=1, 2, 3, \dots$. Different fractions of the particles would then decay with different lifetimes corresponding to these different modes.

If the different modes of decay are considered from the point of view of the motion of different particles constituting the ensemble which correspond to the different initial values of Larmor phase, it is clear that these particles would behave differently because of the difference in initial conditions. But what is most

interesting is that a continuous variation over the initial phase should get mapped into distinct discrete macroscopic ensemble modes of decay ($q=1,2,---$).

Experimental Observation of Multiple Life-times

Experimental investigations of the non-adiabatic leakage of charged particles from a magnetic mirror by Bora et al¹⁰ have shown that the leakage of particles of a given energy E and initial value of the action invariant μ is characterized by more than one lifetime.

In their experiment, the electron current leaking out of the mirror was measured as a function of time, for particles trapped with a particular value of energy and pitch angle. The observations were repeated for different values of magnetic field with constant particle energy and pitch angle.

The analysis of the signal was carried out with a view to obtain estimates of amplitude and e-folding times of exponentials which characterize a given decay curve. In general, it was found that the semi-log plot of the current versus time was not a straight line. To get estimates of the life-time in such cases, the decay signal was fitted to a sum of exponentials.

In general, two decay times with different fractional amplitudes were fitted through the curves. The two life-times observed were found to be exponential functions of confining magnetic fields with the ratio of the exponents lying in the range of 1.8 to 2.3 against the

theoretically predicted value of 2. The values of the exponents were found to vary with magnetic length \propto^{-1} (Fig. 1.2a). However, in certain cases, three decay times were observed for some experimental parameters (Fig. 1.2b). The error bars on the values of the third decay time and corresponding amplitudes are large.

1.3. Bragg-like Reflections of Charged Particles in a Multimirror System

Another ensemble mode behaviour, which the Schroedinger-like equations (1.30), obtained in section (1.1) predict, is one-dimensional interference-like effects and consequent Bragg-like reflections of electrons moving in a spatially periodic magnetic field as that of a multimirror system (a large number of magnetic mirrors joined end to end). It is analogous to quantum interference effect and Bragg reflections arising in the interaction of electrons with the periodic potentials of a crystal lattice⁹.

According to the Schroedinger-like equations, the "quantum conditions" for the Bragg-like reflections are given by

$$2 \int_0^D p_{||} ds = 2\pi \frac{n}{q} \mu$$

(1.32)

where D is the periodic length of the spatially periodic magnetic field, q and n are the different modes and orders.

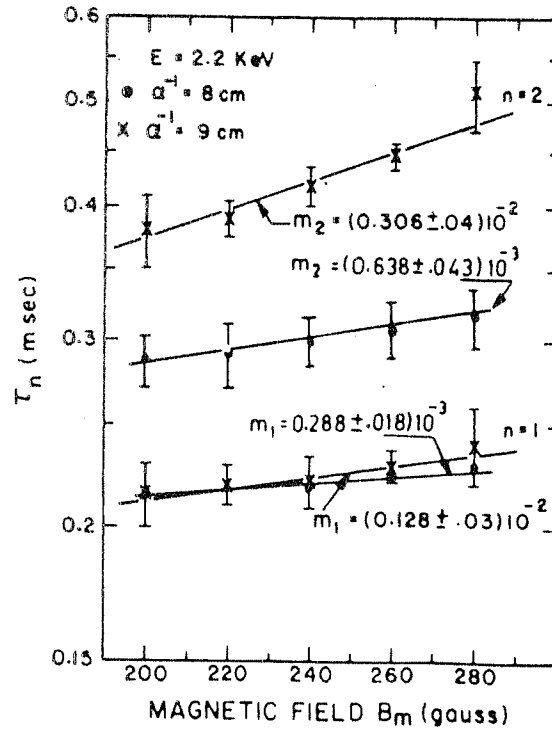


Fig.1.2(a)

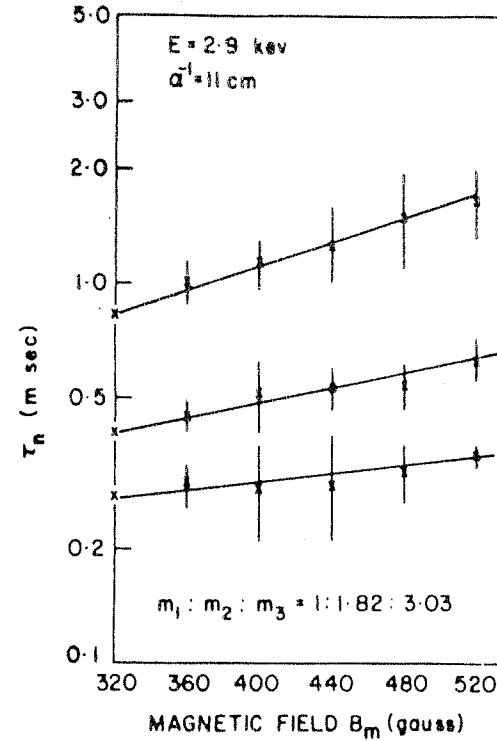


Fig.1.2 (b)

Fig.1.2(a) Dependence of the life times on the magnetic field for two different shapes of the field at mirror throat.

Fig.1.2(b) Three life times as a function of the maximum magnetic field.

If these conditions are satisfied then one should be able to observe these effects. However, for the reflections to be observed the pitch angle of injection should preferably, be close to the loss cone angle so that the non-adiabatic effects are significant.

We now consider a beam (an ensemble) of particles of a given energy E and action μ injected at one end of the multimirror configuration. The pitch angle of the particles is so chosen that the particles are inside the loss cone initially. Particles with different initial values of the Larmor phase would then in general behave differently. The particles may first get trapped in one of the mirrors and may eventually get reflected, or they may get transmitted. In the ideal case, if there is no dispersion in initial μ , according to q th mode of Eq. (1.32) reflection of particles, analogous to the Bragg-reflection, would occur if

$$2 p D \langle \cos \theta \rangle = 2 \pi \frac{\eta}{q} \frac{\frac{1}{2} m v_{\perp}^2}{\Omega}$$

$$\text{or } 4 D = 2 \pi \frac{\eta}{q} \frac{\sqrt{2E/m}}{\Omega} \frac{\sin^2 \theta_0}{\langle \cos \theta \rangle}$$

$$q = 1, 2, 3, \dots$$

$$\eta = 1, 2, 3, \dots$$
(1.33)

θ_0 is initial pitch angle and $\langle \cos \theta \rangle$ is given by

$$\langle \cos \theta \rangle = \frac{1}{D} \int_0^D ds \cos \theta$$
(1.34)

Under conditions of small curvature of field lines, this condition gets simplified into

$$4D = \frac{n}{q} \frac{2\pi}{\Omega} \sqrt{2E/m} \sin\theta \tan\theta \quad (1.35)$$

The equations (1.30) and (1.31) and the consequences (1.32) and (1.33) thereof assume that the initial distribution in μ is a δ -function. In a real experimental situation this is not so. There is always an energy and angular dispersion in the electron beam emerging from an electron gun. Hence, one must examine how the conditions for the occurrence of Bragg-like reflections are affected due to a dispersion in energy and angular dispersion of the electrons.

The number of reflected particles, according to Eq. (1.32), under the conditions of a δ -function in μ , is given by

$$N(B) = N_0 \int \delta(\mu - \mu_0) \delta\left(2 \int p_{||} ds - \frac{2\pi n}{q} \mu_0\right) d\mu$$

where μ_0 is the initial value of action invariant and N_0 is the total number of particles in the injected beam, initially. This gives an integration of

$$N(B) = N_0 \delta\left(2 \int p_{||} ds - \frac{2\pi n}{q} \mu_0\right)_{\mu=\mu_0}$$

which precisely corresponds to the condition (1.32) for a δ -function distribution in μ . For examining the effect of a dispersion in μ , arising out of a dispersion in the pitch angle (still assuming no dispersion in the energy E), a gaussian distribution is assumed instead of

δ -distribution in μ . Now the above relation becomes

$$\begin{aligned}
 N(B) &= N_0 \int e^{-\alpha(\mu-\mu_0)^2} \sqrt{\frac{\alpha}{\pi}} \delta(2 \int p_{||} ds - 2\pi \frac{n}{q} \mu) d\mu \\
 &= N_0 \sqrt{\frac{\alpha}{\pi}} \int d\mu \frac{\delta(\mu-\mu_0)}{\frac{d}{d\mu} [2 \int p_{||} ds - 2\pi \frac{n}{q} \mu]_{\mu=\mu_0}} e^{-\alpha(\mu-\mu_0)^2} \\
 &= \frac{N_0 \sqrt{\alpha/\pi}}{\frac{d}{d\mu} [2 \int p_{||} ds - 2\pi \frac{n}{q} \mu]_{\mu=\mu_0}} \\
 &= \frac{N_0 \sqrt{\alpha/\pi}}{\frac{d}{d\mu} [2 \int \sqrt{2m(E-\mu\Omega)} ds] - 2\pi \frac{n}{q}} \\
 &= \frac{N_0 \sqrt{\alpha/\pi}}{-2\Omega \int \frac{ds}{v_{||}} - 2\pi \frac{n}{q}} \\
 &= \frac{N_0 \sqrt{\alpha/\pi}}{[-\frac{2\Omega}{f_t} - 2\pi \frac{n}{q}]}
 \end{aligned}$$

where $f_t = 1/\int_0^D \frac{ds}{v_{||}}$ is transit frequency which can be defined with the appropriate sign depending on the direction of motion of the particles and Ω is cyclotron frequency. We see from the above that the number of reflected particles $N(B)$ as a function of the magnetic field strength "blows up" (that is, becomes very large) when the following condition is satisfied

$$2|\Omega| = 2\pi \left(\frac{n}{q}\right) |f_t|$$

or

$$2|\Omega| = \frac{n}{q} |\omega_c| \quad (|\omega_c| = 2\pi |f_t|)$$

(1.36)

In the approximation of small curvature of magnetic field

lines, the above condition can be rewritten as

$$2D = +\frac{n}{q} \frac{2\pi}{\Omega} \sqrt{2E/m} \cos \theta \quad (1.37)$$

Any dips observed in the transmitted currents as the magnetic field is varied for a given energy of the beam and pitch angle of injection could be identified with the relation (1.36) with different values of orders (n) and modes (q).

1.4. Survey of Theoretical, Numerical and Experimental Investigations of Motion of Charged Particles in Spatially Periodic Magnetic Field

It is pertinent to note here that the transmission of an electron beam through a periodic magnetic field structure has been investigated by several other authors in the past. The studies were mostly motivated by the possibilities of using such structures in plasma confinement, plasma stability and construction of high power masers etc¹¹⁻¹⁷. However, as we shall see below, the approaches in all these investigations, both theoretical and experimental, have been different from the one described in para 1.3. There are theoretical studies of resonance interaction of electron beams with periodic structures of magnetic field^{18, 19, 22, 23}, experimental studies to verify the predictions following from the above studies^{18, 20, 22, 23, 24} and numerical simulation of the same phenomenon²¹. In the next few paragraphs we carry out a survey of some of the earlier theoretical, numerical and experimental

investigations, which are relevant to the investigations carried out by us in the present work.

One of the earliest investigations, both theoretical and experimental, of the behaviour of charged particles in a periodic magnetic field structure has been carried out by Fedorchenko and others in 1959 at the Acad. of UKSSR¹⁸. In this work the authors have found that during the motion of electron in a magnetic field which is constant in time but modulated weakly in the longitudinal direction, under certain conditions a "resonance relation" exists between the velocity of the electron, the fixed component of the magnetic field and the period of the spatial modulation. As a result of this resonant interaction the magnetic moment of the electron is no more conserved and the longitudinal energy gets converted into transverse energy.

The above effect has been regarded as a case of parametric resonance. An axially symmetric system of magnetic field is considered

$$H_x = -\frac{1}{2} h \nu x \cos(\nu z)$$

$$H_y = -\frac{1}{2} h \nu y \cos(\nu z)$$

$$H_z = H_0 + h \sin(\nu z)$$

(1.38)

where H_0 is the fixed component of the magnetic field, h is the amplitude of the spatial variation and $\nu = 2\pi/L$, L being the spatial period of the field variation. It is assumed that $h \ll H_0$.

The equations of motion for the electron in this field

are written as

$$\begin{aligned}\ddot{x} &= \Omega \left[\dot{y} \left(1 + \frac{h}{H_0} \sin \nu z \right) + \frac{1}{2} \frac{h}{H_0} \dot{z} \nu y \cos \nu z \right] \\ \ddot{y} &= \Omega \left[-\frac{1}{2} \frac{h}{H_0} \dot{z} \nu x \cos \nu z - \dot{x} \left(1 + \frac{h}{H_0} \sin \nu z \right) \right] \\ \ddot{z} &= \Omega \frac{\nu}{2} \frac{h}{H_0} (x \dot{y} - \dot{x} y) \cos \nu z\end{aligned}$$

(1.39)

Neglecting the change in the longitudinal velocity

($\dot{z} = V_{||} = \text{constant}$) and introducing the notation $U = x + iy$ from the above equations the authors obtain

$$\ddot{U} + i \Omega \left(1 + \frac{h}{H_0} \sin \nu z \right) \dot{U} + \frac{1}{2} \frac{h}{H_0} \nu V_{||} \cos \nu z U = 0$$

Further using the substitution $W = U e^{\frac{i}{2} \frac{\Omega}{V_{||}} \int_0^z \left(1 + \frac{h}{H_0} \sin \nu z \right) dz}$

a Mathieu's equation has been obtained for W , a quantity proportional to the larmor radius of the electron.

$$\frac{d^2 W}{dz^2} + \frac{\Omega^2}{4 V_{||}^2} \left(1 + \frac{2h}{H_0} \sin \nu z \right) W = 0$$

(1.40)

From the properties of the unstable solutions of this equation it is predicted that, in the neighbourhood of values of $\Omega/V_{||}$ equal to $\nu, 2\nu, 3\nu, \dots$, the transverse energy of the electron would grow exponentially with varying amplitudes. In contrast with the other known resonances, where the time varying magnetic field changes the total energy of the particle^{25, 26}, in the case of a spatially periodic field the total energy has to be conserved and hence the energy of the transverse motion can increase only at the expense of the longitudinal energy.

The authors¹⁸ had also carried out experiments to verify the above predictions. An electron beam was passed through a spatially periodic structure. The period L was equal to 7 cms. and the number of periods was equal to 5.5. The fixed magnetic field was about 200 oerst. and the maximum value of h was 60 oerst.

The longitudinal energy of the electron beam, initially with an energy equal to 2 KeV, was measured with a retarding potential analyzer. The current versus retarding potential plots as recorded by the detector at various values of the modulating field are shown in fig. 1.3a. By a comparison of these plots the authors conclude that the longitudinal energy of electrons is actually reduced when they pass through the modulated magnetic field. The above effect has been observed only when the transit frequency ω_t is equal to Ω .

From the above current versus retarding voltage plots, it was seen that as the modulating field h is increased the velocity distribution over $V_{||}$ exhibits maxima which are displaced in the direction of lower $V_{||}$. The mean energy associated with the transverse motion shows an increasing tendency as h is increased (Fig. 1.3b). Experiments were also done with a movable retarding potential analyzer, which show the dependence of perpendicular energy on the number of periods of the system n , traversed by the electrons (Fig. 1.3c).

It should however be added here that inspite of the fact that the authors have carried out experiments in a

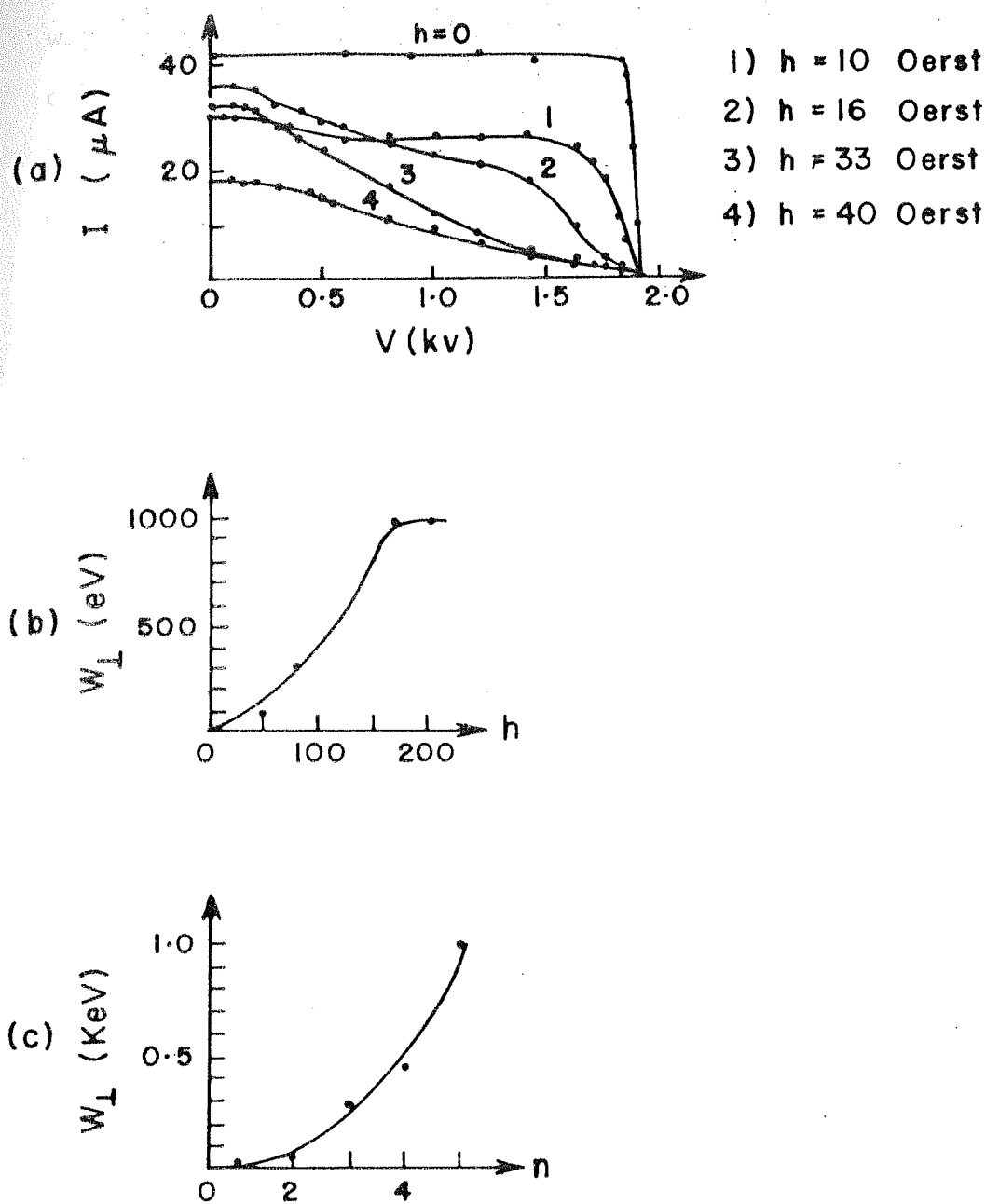


Fig.1.3 (a) The analyzer current as a function of retarding potential at an anode voltage $V_0 = 2$ kV and a magnetic field $H_0 = 136$ oerst for various values of the modulating field h .

(b) The transverse energy as a function of magnitude of the modulating magnetic field h with $V_0 = 2$ kV and $H_0 = 136$ oerst.

(c) The transverse energy as a function of the number of periods n , traversed by the electron with $V_0 = 2$ kV and $H_0 = 136$ oerst.

wide range of modulation factors, from 7% to 30%, they have observed only one resonance i.e., $\omega_t = \Omega$, whereas with a 30% modulation factor one would expect to register many more orders, after the electron beam traverses 5.5 periods.

Sinelnikov, along with two of the authors of the above mentioned paper has also carried out theoretical investigations¹⁹ of the motion of a charged particle in a spatially modulated field. Nonlinear equations of motion of the particle in such fields were obtained and using asymptotic methods under the assumption that the modulation factor is small, the equations are solved. It has been shown that the magnetic moment of the particle moving in the modulated field is not conserved, when the condition $\Omega = \omega_t$ is satisfied. The energy of the longitudinal motion goes over into energy of the Larmor rotation, or vice versa, depending upon the relation of the phases of the Larmor rotation and the external periodic action of the field on the moving particles.

Experiments have been carried out by the same authors²⁰ to verify the possibility of accumulating particles in a mirror trap with its central region modulated spatially. The authors have reported accumulation of electrons in such a system accompanied with the formation of a negative space charge in the volume of the trap when the condition $\Omega = \omega_t$ is satisfied.

Numerical simulation of the transit of charged particles through a spatially modulated magnetic field has been carried out by Laing and Robson²¹. A quantity ξ is

defined which is equal to the ratio of rotational to the parallel energy of the charged particle. The dependence of this quantity on various parameters like ω_t/Ω , n the number of mirrors traversed by the particle, etc., are obtained.

The equations of motion are written in cylindrical polar co-ordinates $(r, \theta$ and $z)$. The magnetic field is taken to be $H(H_r, 0, H_z)$, where $H_r = -1/2 r H_0 \partial f / \partial z$ and $H_z = H_0 f(z)$. The spatial variation in the magnetic field is $f(z) = 1 + h \sin z \cdot \lambda / 2\pi$ (λ being the mirror length) is taken as the unit of length. A new variable $\tau = 1/2 \Omega t$ is introduced where $\Omega = \frac{eH_0}{mc}$ and P_θ is replaced by $1/2 mC$.

The equations of motion under the above conditions thus become

$$\begin{aligned} \frac{d^2 \lambda}{d\tau^2} &= \frac{c^2}{\lambda^3} - \lambda f^2 \\ \frac{d^2 z}{d\tau^2} &= (c - \lambda^2 f) \frac{df}{dz} \\ c &= \lambda^2 \left(\frac{d\theta}{dz} + f \right) \end{aligned} \quad (1.41)$$

These equations have a first integral

$$\left(\frac{d\lambda}{d\tau} \right)^2 + \left(\frac{dz}{d\tau} \right)^2 + \left(\frac{c}{\lambda} - \lambda f \right)^2 = \mathcal{V}^2 \quad (1.42)$$

where parameter \mathcal{V} is related to the total velocity v of the particle by

$$\mathcal{V} = \frac{2v}{\Omega} \quad (1.43)$$

The condition for the resonance $\Omega = \omega_t$ thus becomes $\mathcal{V} = 2$.

Using the above equations a single equation is written

$$\frac{d^2 \lambda}{dz^2} = \frac{(1 + (\frac{dr}{dz})^2) (c - \lambda^2 f) (\frac{c}{\lambda^3} + \frac{f}{\lambda} - \frac{dr}{dz} \cdot \frac{d\lambda}{dz})}{v^2 - (\frac{c}{\lambda} - \lambda f)^2} \quad (1.44)$$

The boundary conditions for the above equation are taken to be

$$r = r_0, dr/dz = 0 \text{ at } z=0$$

The equation is solved numerically and the energy transfer efficiency ξ is plotted against v for passage of particle through different number (n) of wavelengths of modulations. Some of the typical dependences obtained are shown in figs. 1.4a, b. Fig. 1.4a shows details of the resonance for values of n upto 10 and modulation coefficient $h = 0.05$. Fig. 1.4b shows similar results for $h = 0.025$. The main features as pointed out by the authors are

1. There is a pronounced resonance for $v=2$ i.e. $\Omega = \omega_t$.
2. As n is increased, the height of the resonance increases at first rapidly (approximately as n^2) and then more slowly.
3. The effect of increasing n is to increase the sharpness of the resonances and to shift the peak to a value of v somewhat greater than 2.

The authors explain the shift in the resonance as that due to the coupling between the transverse and axial velocity components through the conservation of energy. The axial velocity decreases as the particle moves through the

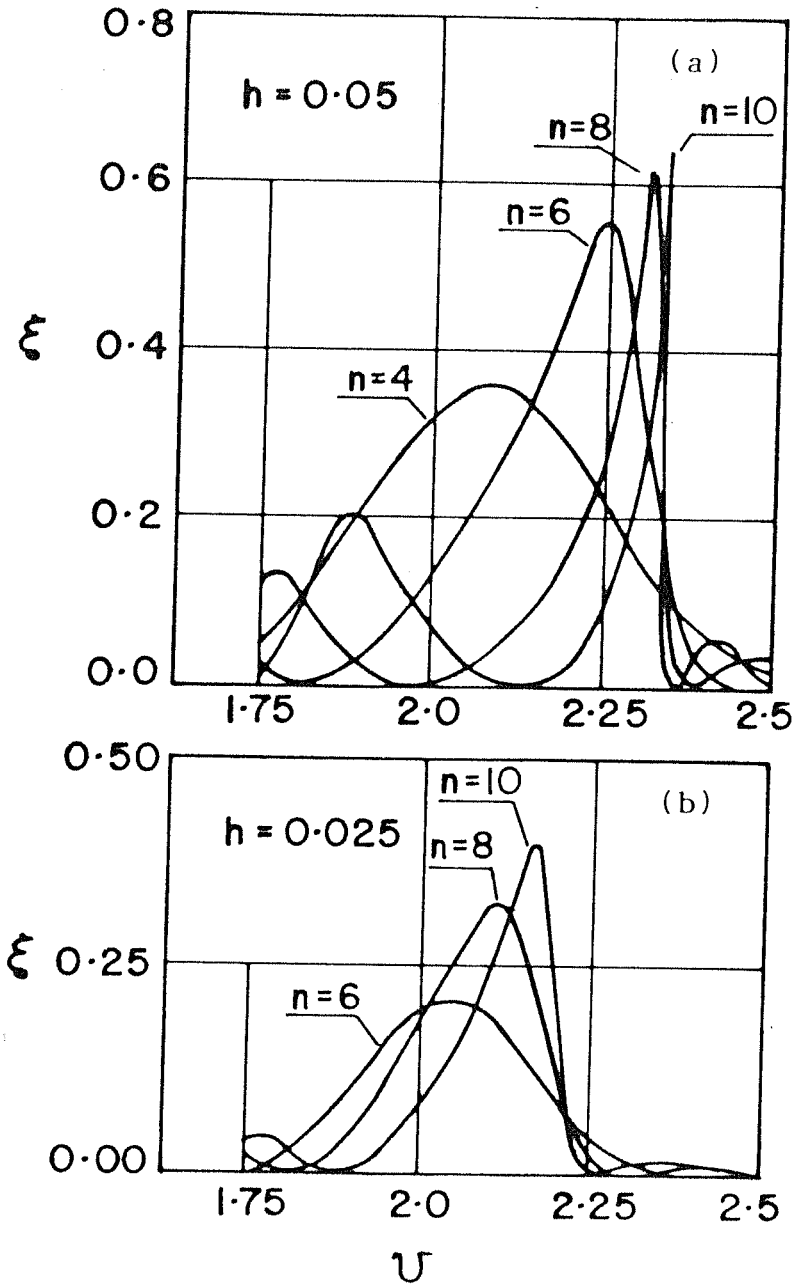


Fig. 1.4 ξ as a function of U for values of n upto 10 and $h=0.05$ and 0.025 respectively.
a, b

modulated field, and hence by taking \mathcal{V} slightly greater than 2 this tends to draw the particle into resonance, and to increase the total effect of n periods.

The authors have also suggested that since it is not possible to satisfy the resonance condition during passage through a large number of mirrors, better efficiency could be attained by progressively decreasing the wavelength of the modulation, thus increasing the period of the resonance interaction.

It is however necessary to point out here that neither the theory nor the observations provide any satisfactory explanation for the sharpening of the resonance and the shifting of the resonance to higher values of \mathcal{V} with the increase in the number of mirrors traversed by the particle.

The results reproduced hereinabove raise yet another question. The resonance interaction studied in this paper is identical to the one investigated in the work of Fedorchenko¹⁸, wherein it was found that the motion of particles in such a system is described by Mathieu's equation. It is also known that in such a case the solutions are unstable whenever the conditions $\Omega = n\omega_t$ are satisfied, when the perpendicular energy should grow exponentially. However, the numerical calculations yield no other resonances apart from $\Omega = \omega_t$.

Further even in this resonance $\Omega = \omega_t$, it is known from the theory of Mathieu's equations that the width of resonance region increases proportional to h , the modulation factor. A comparison of the plots, in figs. 1.4a and 1.4b

wherein the resonance plots for two different modulation factors 0.05 and 0.025 are reproduced, reveal the opposite character. The above controversial results only point out the necessity for more exact theoretical investigations.

Some more theoretical and experimental investigations have been carried out to study the motion of a charged particle in spatially periodic helical magnetic fields. These studies by Richard C. Wingerson²² and R.A. Demrikhanov et al²³ have also used the resonance growth of the transverse velocity at the expense of longitudinal energy to trap electrons, injected from outside the mirror. These experiments²³ report observation of resonance interaction at $\Omega = \omega_t$ and $2\Omega = \omega_t$. The magnetic fields produced in these systems have an azimuthal component also. The resonance interactions were observed only in those cases in which the direction of the Larmor gyration of the electrons coincided with the direction of current in the helical winding.

Recently Tetsu Mieno et al²⁴ have reported the results of their investigations of the motion of an ion beam in a multiple mirror configuration of magnetic field. The authors have carried out numerical simulation on a computer, and experiments on a double plasma machine, incorporated with a periodic magnetic field structure. Under conditions of spatial ion cyclotron resonance i.e. $\Omega_i = \omega_t$, they have observed a drastic transfer of the beam energy into transverse direction both in the numerical simulations and in the experiments.

In an axially symmetric spatially periodic magnetic field structure with

$$B_r = b \gamma r/2 \sin \gamma z, \quad B_\theta = 0, \quad B_z = B_0 + b \cos \gamma z$$

where $\gamma = 2\pi/L_c$, L_c being the mirror length and $b \ll B_0$, the equation of ion beam motion is reduced to the Mathieu's equation as shown earlier¹⁸, by introducing a new function η (assuming that the variations of axial speed v_z is small).

$$\frac{d^2 \eta}{dz^2} + \frac{\pi^2 f_{ci}^2}{V_b^2} \left[1 + \frac{2b}{B_0} \cos \gamma z \right] \eta = 0 \quad (1.45)$$

where

$$\eta = r \exp \left(i\theta + \frac{i\pi f_{ci}}{V_b B_0} \int_0^z B_z dz \right) \quad (1.46)$$

f_{ci} is the ion cyclotron frequency corresponding to the constant magnetic field B_0 .

Under the condition

$$N_0 V_b = f_{ci} L_c \quad (N_0 = 1, 2, 3, \dots) \quad (1.47)$$

the ion Larmor radius increases as a result of resonance.

The efficiency of energy transfer from axial to transverse direction is defined as

$$\xi = \psi_\perp / \psi_b \quad (1.48)$$

where

$$\psi_{\perp} = \frac{1}{2} m_i V_{\perp}^2 ; \quad \psi_{\parallel} = \frac{1}{2} m_i V_{\parallel}^2 \quad (1.49)$$

For carrying out numerical calculations of the ion orbit the equations of motion are expressed by

$$\begin{aligned} \frac{d^2 r}{d\tau^2} &= \frac{c_0^2}{r^3} - \frac{r B_z^2}{B_0^2} \\ \frac{d^2 z}{d\tau^2} &= - \left[c_0 - r^2 \frac{B_z}{B_0} \right] \frac{b v}{B_0} \sin \nu z \\ c_0 &= r^2 \left[\frac{d\theta}{dz} + \frac{B_z}{B_0} \right] = \text{constant} \end{aligned} \quad (1.50)$$

where τ is the normalized time, $\tau = \pi f_{ci} t$. The solutions of these equations obtained for $L_c = 10$ cms, the number of mirrors $N=6$, the mirror ratio $R_m = 1.3$, f_{ci} (at $B_0 = 2.7$ KGauss) = 107 KHz and the initial radial position $r_0 = 1.0$ cm. are shown in fig. 1.5a,b. The figures show the radial position r of the beam, the efficiency of energy transfer ξ and the axial derivative of ψ_{\perp} , $\frac{d\psi_{\perp}}{dz}$ respectively as functions of Z/L_c . Fig. 1.5a corresponds to the case of exact resonance conditions $V_b = f_{ci} L_c$ and Fig. 1.5b shows the same dependences when the resonance condition is disturbed by nearly 12% i.e. $V_b \approx 1.12 f_{ci} L_c$. From these figures it is seen that when the exact resonance condition is satisfied, the resonance saturates at $z = 4 L_c$ and beyond that point ξ decreases spatially. In the other case when there is a small mismatch i.e., $V_b \approx 1.12 f_{ci} L_c$ the saturation is not found and ξ increased upto 0.64 in the range $Z = 6 L_c$. The authors explain the results in the

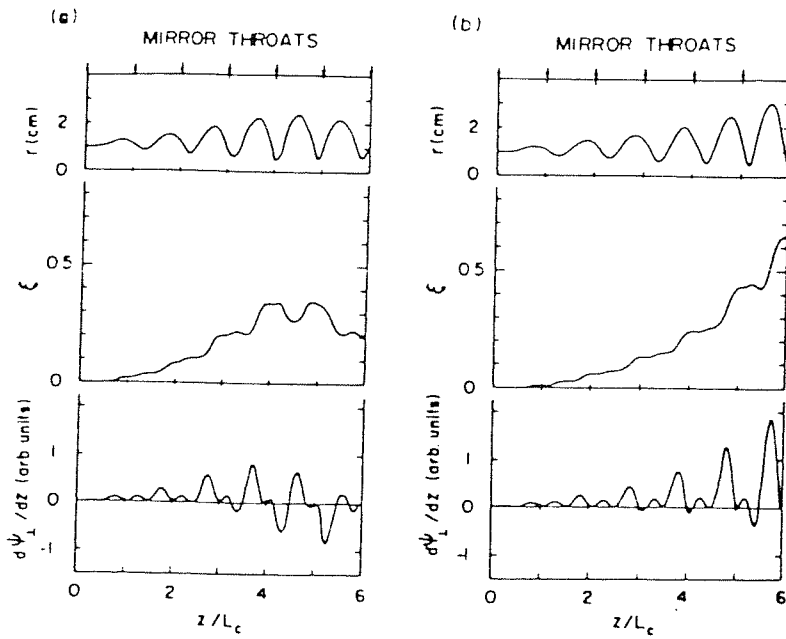


Fig. 1.5 Radial ion motion, energy transfer coefficient and axial derivative of the transverse energy, $d\psi_L/dz$, in a multiple mirror with cell length $L = 10$ cm, cell number $N = 6$, mirror ratio $R = 1.3$. At the ion injection point $z = 0$, the radial position of the ion is $r = 1.0$ cm. Initial beam energy is $(a) \psi_b = \psi_{bR}$ ($V_b = f L_c$) and (b) $\psi_b = 1.25 \psi_{bR}$.

following manner.

When the exact resonance condition is satisfied at $z=0$, V_z decreases with an increase in z , as a result of which the beam does not remain in the resonance for long and hence a saturation is noticed at $z = 4 L_c$. For $V_b = 1.12 f_{ci} L_c$, the rate of growth of ψ_1 is smaller and hence no saturation is noticed till the beam passes through 6 mirrors when ξ increases upto 0.64. This is because a beam with V_b a little larger than $f_{ci} L_c$ remains around the resonance conditions in a wider range of Z , being accompanied with an increase in ξ along the axial direction. However, the authors do not provide an explanation for the decrease in ξ after the saturation occurs.

The experimental investigations were carried out in a double plasma type machine. A multiple mirror configuration of magnetic field is produced by using 6 iron rings under a uniform magnetic field. The mirror length L_c was equal to 10 cms, mirror ratio equal to 1.2-2 depending on B_0 (1-4 KGauss).

The magnetic field B_0 is kept constant at 2.7 KGauss and the beam energy is varied over the range 0-60 eV. In order to look for the spatial ion cyclotron resonance, the ion beam current densities are measured with grided analyzers in the regions of the entrance (Fig. 1.6a) and exit (Fig. 1.6b) of the multiple mirror configuration. The transverse current measured at exit is shown in Fig. 1.6c. Around $\psi_b = 23$ eV, the $I_{c \parallel}$ is found to decrease drastically and correspondingly the transverse current $I_{c \perp}$

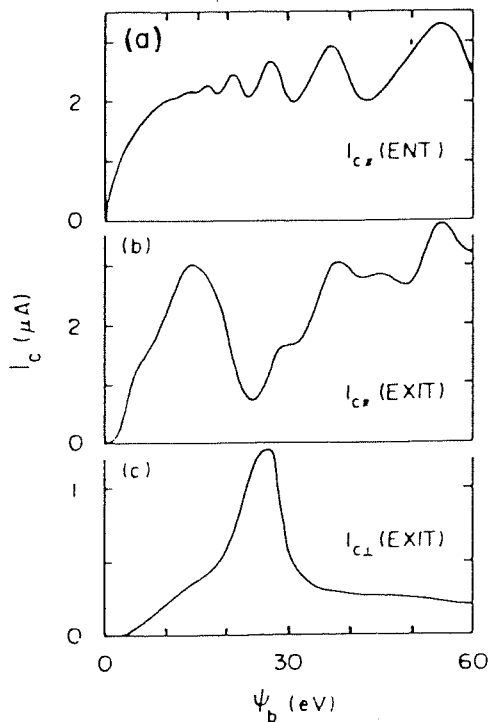


Fig. 1.6 (a) Axial ion current $I_{c^{\parallel}}^{\parallel}$ at the entrance position near the axis (13 cm upstream from the first mirror point).
 (b) Axial ion current $I_{c^{\parallel}}^{\parallel}$ at an exit position of the multiple mirror near the axis (10 cm downstream from the last mirror point).
 (c) $I_{c^{\perp}}^{\perp}$ at the same position of (b) as a function of the injected beam energy ψ_b . B_0 is fixed at 2.7 K Gauss.

increases and peaks around the same value.

The ion energy distributions were obtained by differentiating the collector current versus voltage characteristics of the analyzer. The axial energy distributions $F_{\parallel}(V_c)$ are shown at the last mirror point (Fig. 1.7a). For Ψ_b a little above the resonance beam energy 23 eV, which corresponds to the spatial ion cyclotron resonance, $F_{\parallel}(V_c)$ is found to be deformed from a shifted Gaussian type distribution, producing a lower energy component. Fig. 1.7b shows the transverse energy distribution $F_{\perp}(V_c)$ measured at the same position of the analyzer. For Ψ_b a little above 23 eV a high energy tail is noticed in this plot. Around the resonance condition the $F_{\parallel}(V_c)$ is found to have two clear peaks. The peak on the higher side of the energy corresponds to the non-resonant part of the beam ions, which have almost the same energy as the injected beam energy and the peak corresponding to the lower energy is attributed to the resonant ions.

1.5. Discussion

In the previous sections of this chapter we have reviewed the theoretical, numerical and experimental works on the behaviour of charged particles in an inhomogeneous magnetic field and also more specifically in a spatially periodic magnetic field structure. From this overview it is seen that these works have led to important observations and conceptual information on particle interaction with such magnetic field structures. However, in spite of all these

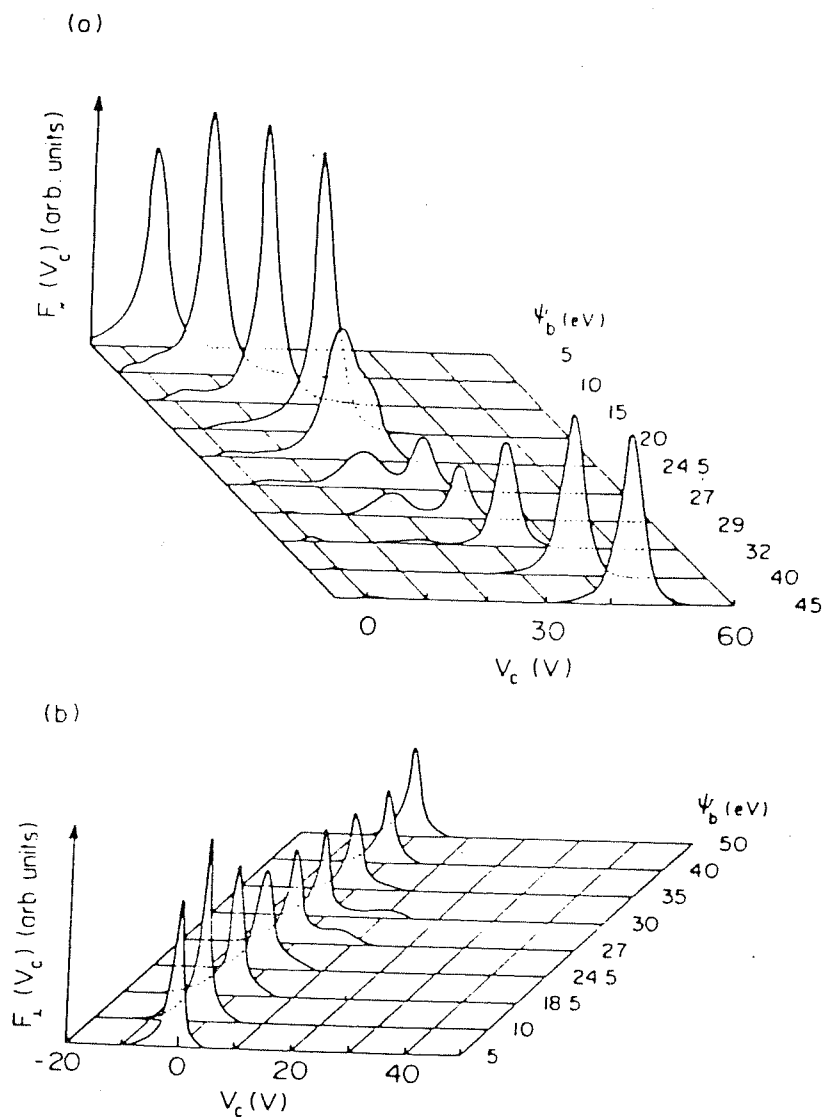


Fig. 1.7 Variations of (a) axial energy distribution (b) transverse energy distribution near the axis at the exit position of the multiple mirror as function of the injected beam energy. $\psi_b = 23$ eV corresponds to the resonance condition.

efforts, we have also noticed that there remain many unresolved questions.

In the theoretical considerations of a multimirror system, reviewed in the previous section, the authors have assumed the modulation factor to be very small compared to unity and thereby obtain a Mathieu's equation to describe the motion of charged particles in a spatially periodic magnetic field. The unstable solutions of this equation are obtained under the fulfilment of the condition $\Omega = n\omega_c$. However, from the theory of nonlinear oscillatory systems we know that resonances can, in general, occur at²⁷

$$\ell \Omega = n \omega_c \quad (1.51)$$

where both ℓ and n are integers. The Mathieu's equation obtained under various assumptions, as described earlier, gives unstable solutions corresponding to $\ell = 1$ only. The experiments of Demirkhanov²³ have recorded a resonance at $\ell = 2$ also.

The theoretical considerations, described in section (1.3) predict the occurrence of Bragg-like reflections in a periodic magnetic field under the conditions

$$2D = 2\pi \frac{\eta}{q} \frac{\mu}{\rho_{||}}$$

in the case of monoenergetic electron beam with no angular dispersion or at

$$2q\Omega = n\omega_c$$

in the case of a beam with an initial dispersion in μ .

It is interesting to note that the relations $2q\Omega = n\omega_c$

are contained in the relations $l\Omega = n\omega_t$ corresponding to the even values of l .

The observation of the various orders and modes and further checking the dependence of these interactions on the experimental parameters like the magnetic field, beam energy and the injection angles are the challenges which have been accepted by us for which a multimirror machine was set up, the details of which are given in the next chapter.

CHAPTER II

Experimental Arrangement

The objective of the present experimental work, as described earlier, was to study the motion of charged particles in a spatially periodic magnetic field and to see whether the theoretically predicted Bragg-like reflections of charged particles do indeed occur whenever the corresponding "quantum" conditions are satisfied. The occurrence of such reflections would result in a reduction of the particle flux transmitted through the multimirror system. The primary requirements for carrying out an experiment to observe these effects are high vacuum, a particle beam with a minimum energy and angular dispersion, a periodic magnetic field with an appropriate periodic length and a sensitive diagnostic system.

This chapter describes the experimental system designed and constructed to fulfil the above objectives. The experimental set up can be broadly divided into the following sections:

1. Vacuum System 2. Magnetic Field system 3. Electron Gun 4. Diagnostics

The photograph and the schematic of the experimental device are shown in figs. 2.1 and 2.2 respectively.

2.1. Vacuum System

The vacuum chamber of 310 cms in length and 27.0 cm in diameter, accomodating 17 mirrors with a mirror length of 17 cms, was used for carrying out the experiment. The vacuum system was constructed entirely from 304 stainless steel. At the ends of the experimental chamber there are two Tees which form junctions to the vacuum pumps and end ports. In order to obtain desired small mirror lengths, the internal diameter of the field coils was made close to the outer diameter of the experimental chamber. For this purpose the two ends of the experimental chamber were connected with Tee junctions with the help of rotatable flanges, made in two semicircles and fitted in place after the insertion of the magnetic field coils. The gap available between the adjacent coils is less than 15 mm, as a result of which no provisions could be made for additional ports along the length of the chamber. The lower ports of the Tee junctions were connected to Diffstak pumps, which have a pumping speed of 700 litres per second and are capable of giving an ultimate vacuum equal to 3×10^{-8} torr. Two rotary pumps EDM-20 with speeds $20.5 \text{ m}^3/\text{hr}$ were used in conjunction with the Diffstak pumps. The baffle valves of the Diffstak pumps

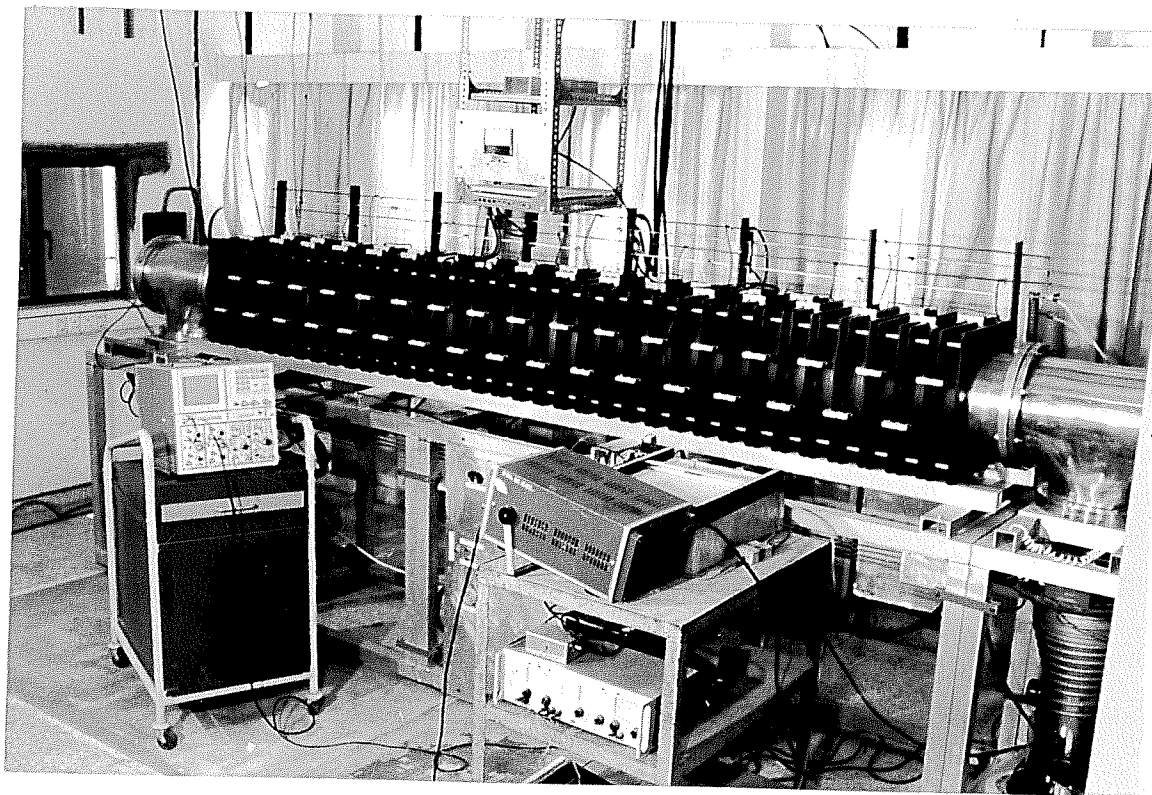


Fig. 2.1 Multimirror machine

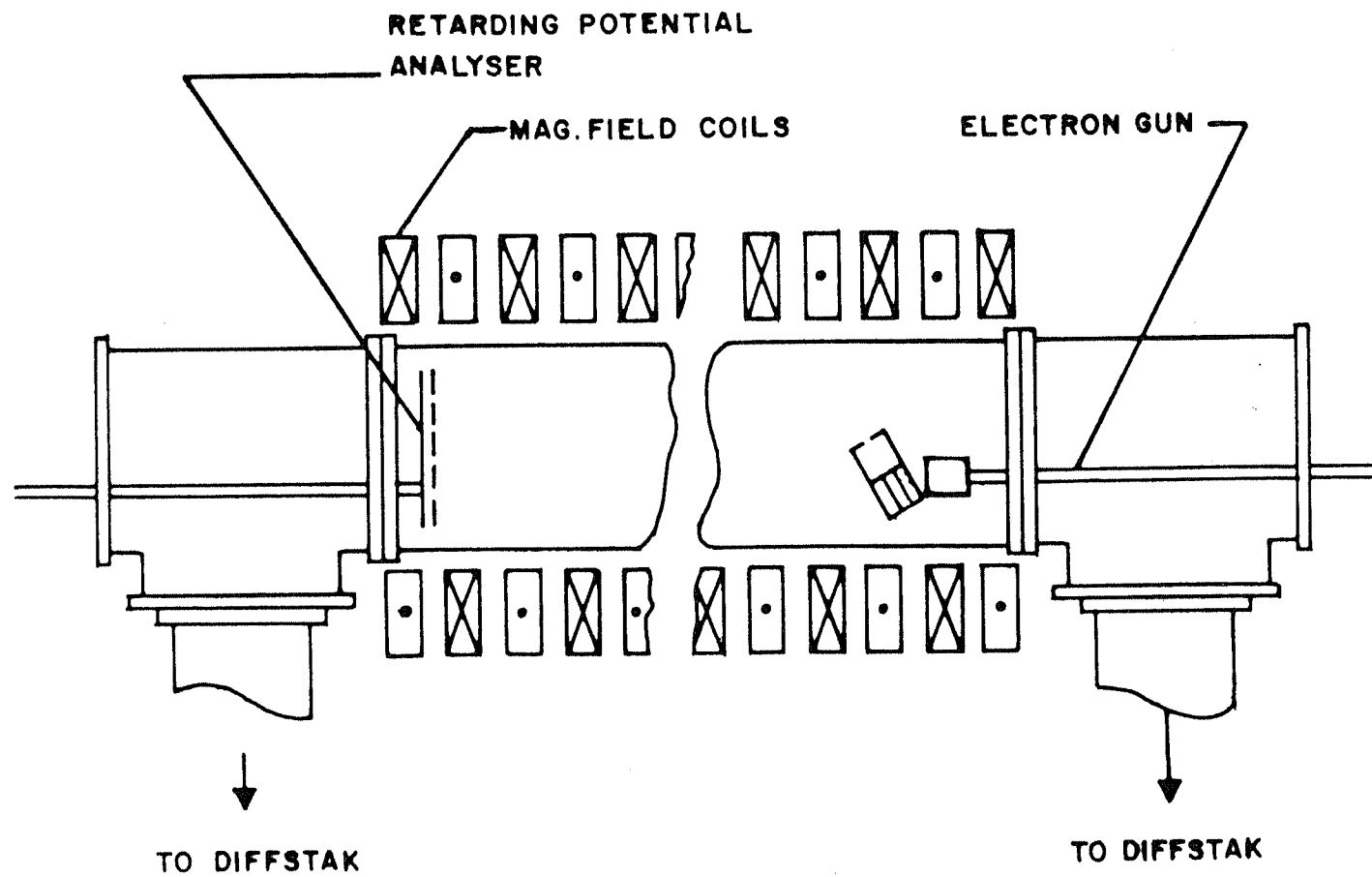


Fig.2.2 Schematic of the experimental device

and the backing and roughing valves in the forevacuum pumping line were operated pneumatically. The control panel, the schematic of which is shown in fig. 2.3, using electro-pneumatic valves was incorporated into the vacuum system for the automatic control of the pumping procedures and also as a protection mechanism against power failures and thus enabled non-stop pumping of the system. The entire system was pumped down to a pressure better than 3×10^{-7} torr. The pressure in the chamber is measured with the help of a Ionivac ionization gauge. The mean free path of the electron neutral collision at this pressure is found to be two orders of magnitude greater than the length of the experimental chamber thus eliminating the possibilities of beam losses due to collisions. The two end ports of the Tee junctions carried flanges, on which were mounted viewing ports, electrical feedthroughs for connections to the electron gun and the diagnostics, vacuum gauge heads and Wilson feedthroughs.

2.2. Magnetic Field System

The design of the magnetic field coils becomes complicated by the fact that for the observations of the lowest orders and modes of the Bragg-like reflection, the mirror length will have to be comparable to the Larmor radius of the electron. Initially attempts were made to produce the multimirror magnetic field configuration by placing rings made of high permeability material inside a homogeneous magnetic field, as has been attempted in some

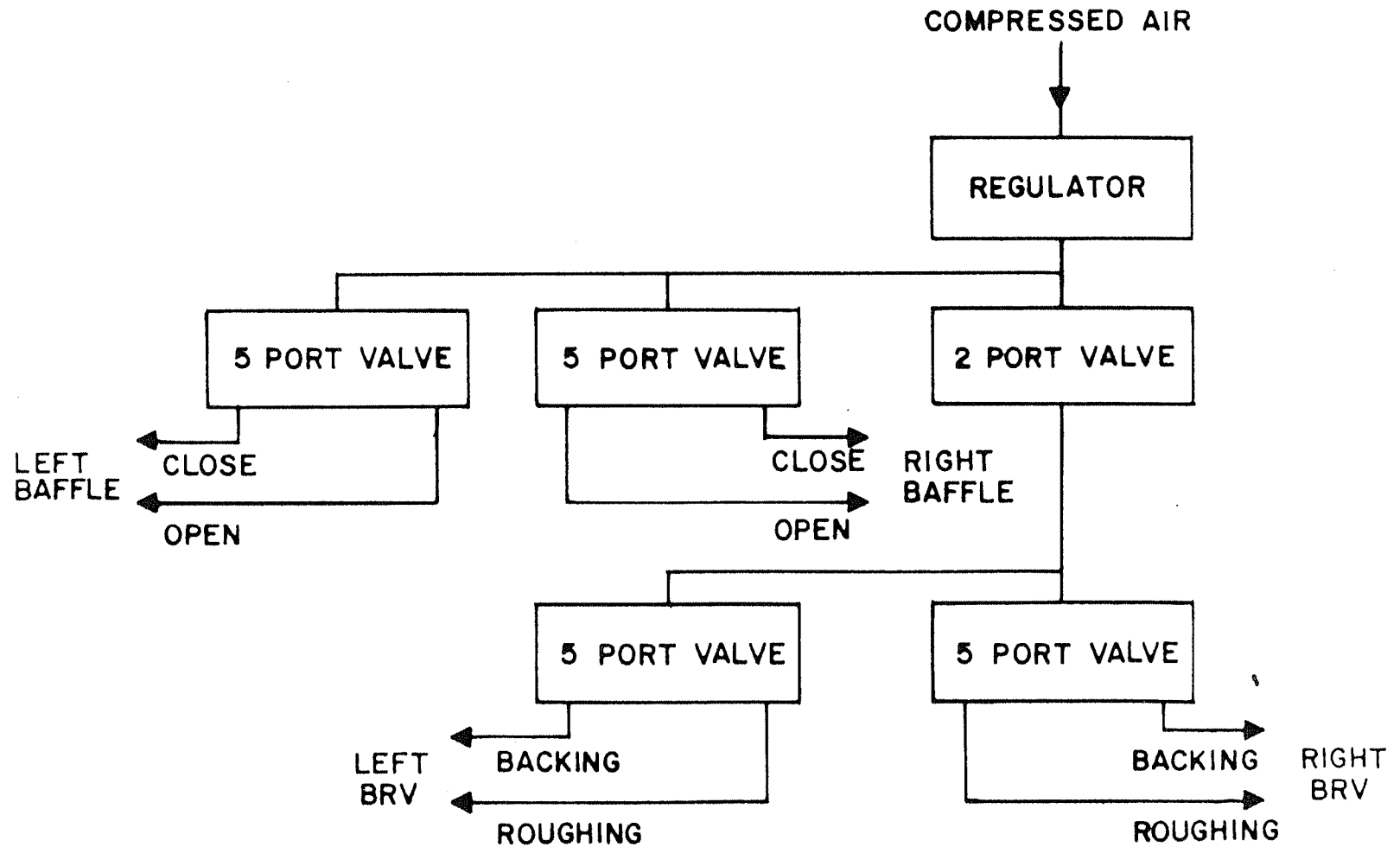


Fig. 2.3 Block diagram of electropneumatically controlled vacuum system

other experiments^{17,24}. In our experiments it was found that in such a configuration the maximum obtainable mirror ratio along the axis of the system was less than 1.1 whereas we preferred to have a system that could produce mirror ratios upto 1.3.

Initially the idea was to inject the electron beam with such a pitch angle, that it lies just within the loss cone in order to enhance the probability of non-adiabatic interactions with the periodic magnetic field configuration. A mirror ratio of 1.3 would thus necessitate injection of the beam with a pitch angle = 60° , whereas a mirror ratio = 1.1 would need injection at angles near 75° . Such high pitch angles severely limit the magnetic field range over which the transmitted current can be investigated. With an outer diameter of the vacuum chamber equal to 27 cms and a mirror periodic length of about 17 cms, a mirror ratio 1.3 could not be obtained with either iron rings or with coils carrying currents in the same direction. It was therefore, found necessary to use another set of coils numbering seventeen, carrying current in the opposite direction and placed midway between the adjacent even numbered coils numbering 18. We thus have a system of 35 coils of radius 16 cms with alternate coils carrying currents in opposite direction and of unequal amount.

The design of the magnetic field and hence of the current carrying coils producing it was finalised with the help of numerical calculations carried out on a computer. The magnetic field distribution along the axis of the

system with intercoil distance 17 cms, odd numbered coils carrying 1 unit current and the even numbered coils carrying current -0.27, -0.5 and -0.8 in opposite directions is reproduced in fig. 2.4. It is seen that by increasing the current in the even numbered coils it is possible to achieve higher mirror ratios, unlike the design with rings of high permeability materials where it was not possible to vary the mirror ratio. With an increase in current flowing through the even numbered coils, the mirror ratio increases significantly. At the same time the distortions in magnetic field in the region of end coils become significant. Corrections of these distortions were done by making appropriate changes in the currents flowing through the end coils. The numerically obtained dependences of the mirror ratio and magnetic field on the ratio of currents in the even numbered to odd numbered coils and mirror length is shown in table 2.1.

Using the above data it was decided that each of the 35 coils would be made of 112 turns of 12 gauge copper wire wound in 7 layers of 16 turns each. Two power supplies of 0-24 volts capable of giving current upto 240 amperes were used to feed the sets of odd and even numbered coils. Three alternate coils are connected in series and six such combinations were connected in parallel to a system of bus bars. In the case of 17 even numbered coils, an additional resistance equivalent to the resistance of the coil was connected at the end, to complete sets of 3 coils. In order to obtain the necessary ratios of currents in the two sets

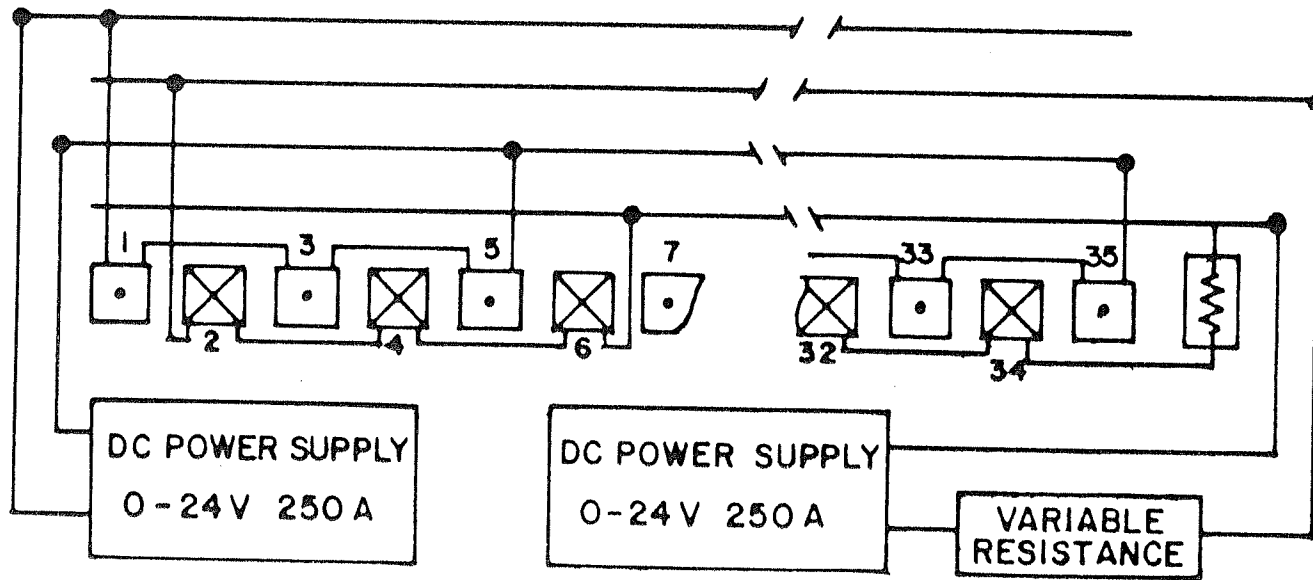


Fig.2.4 Block diagram of power connections to magnetic field coils

of coils, a resistance box was used in series in the circuit of the even numbered coils. The resistance box contains 7 coils made of 6 mm dia stainless steel rod and immersed in transformer oil. By choosing appropriate number of these stainless steel shunts, it is possible to adjust the current ratios and thereby achieve different mirror ratios. The electrical connections of the field coils are shown in fig. 2.5.

The distribution of magnetic field along the 35 coil system was obtained experimentally in the following manner. Alternating currents of known amplitudes and in opposite phases were passed through the two sets of coils. A pick up coil was moved around a guiding wire stretched along the length of the system, with the help of a motor and pulley system. The output from the pick up coil was rectified and this voltage was plotted as a function of distance on an X-Y chart recorder. Three different plots, for different ratios of current flowing in the two sets of coils obtained by the above method, are shown in fig. 2.6. The axisymmetry of the magnetic field, produced by the system was tested by moving the pick up coil at a radial distance of 9 cms from the axis and repeating the experiment at different points along the circumference of the system. Necessary corrections in the positions of coils were made to minimize the distortions in the axisymmetry of the magnetic field. Similar plots were also obtained at different radial distances from the axis in order to get the values of mirror ratios at different radial distances.

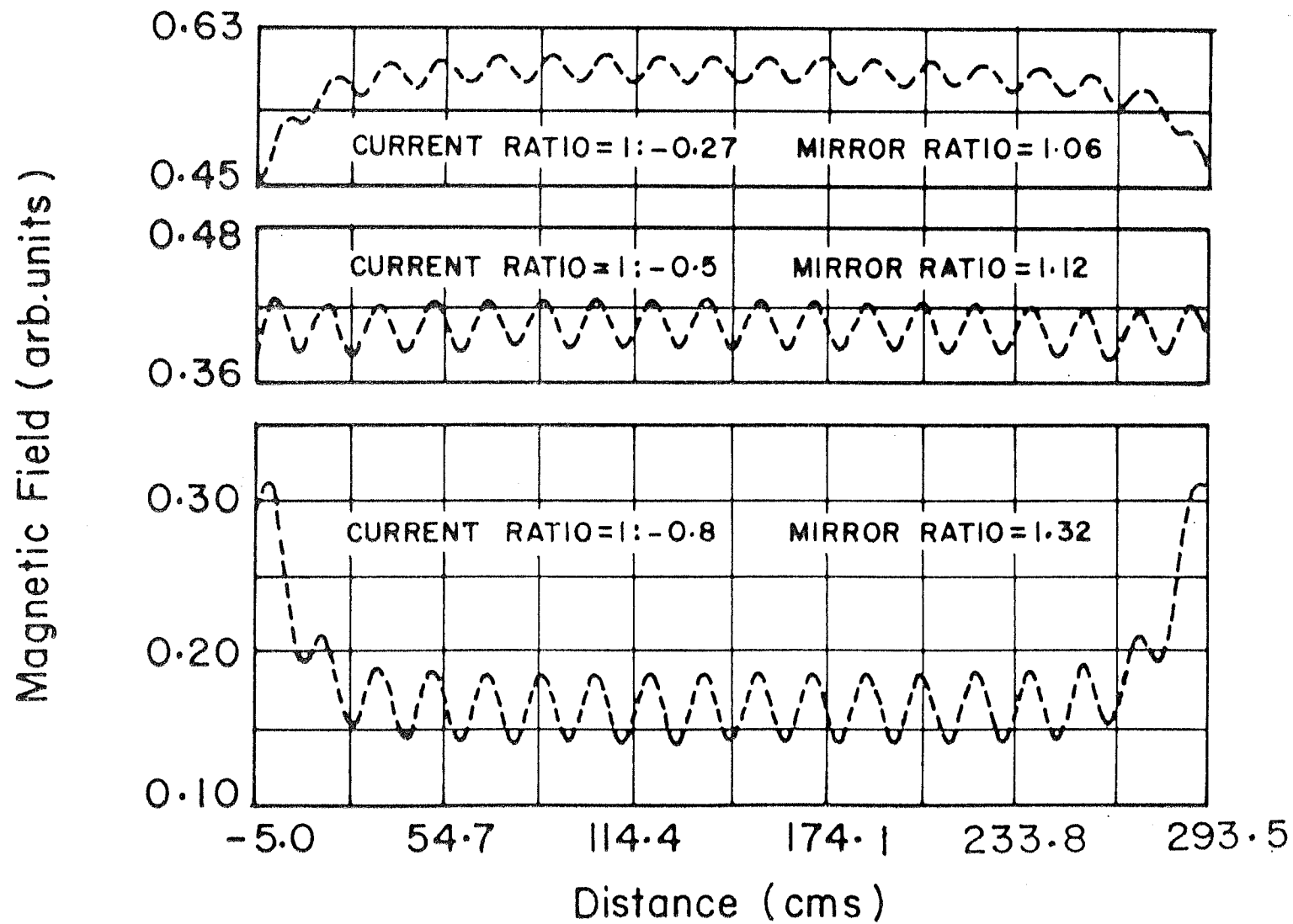


Fig. 2.5 Computer plots of magnetic field distribution

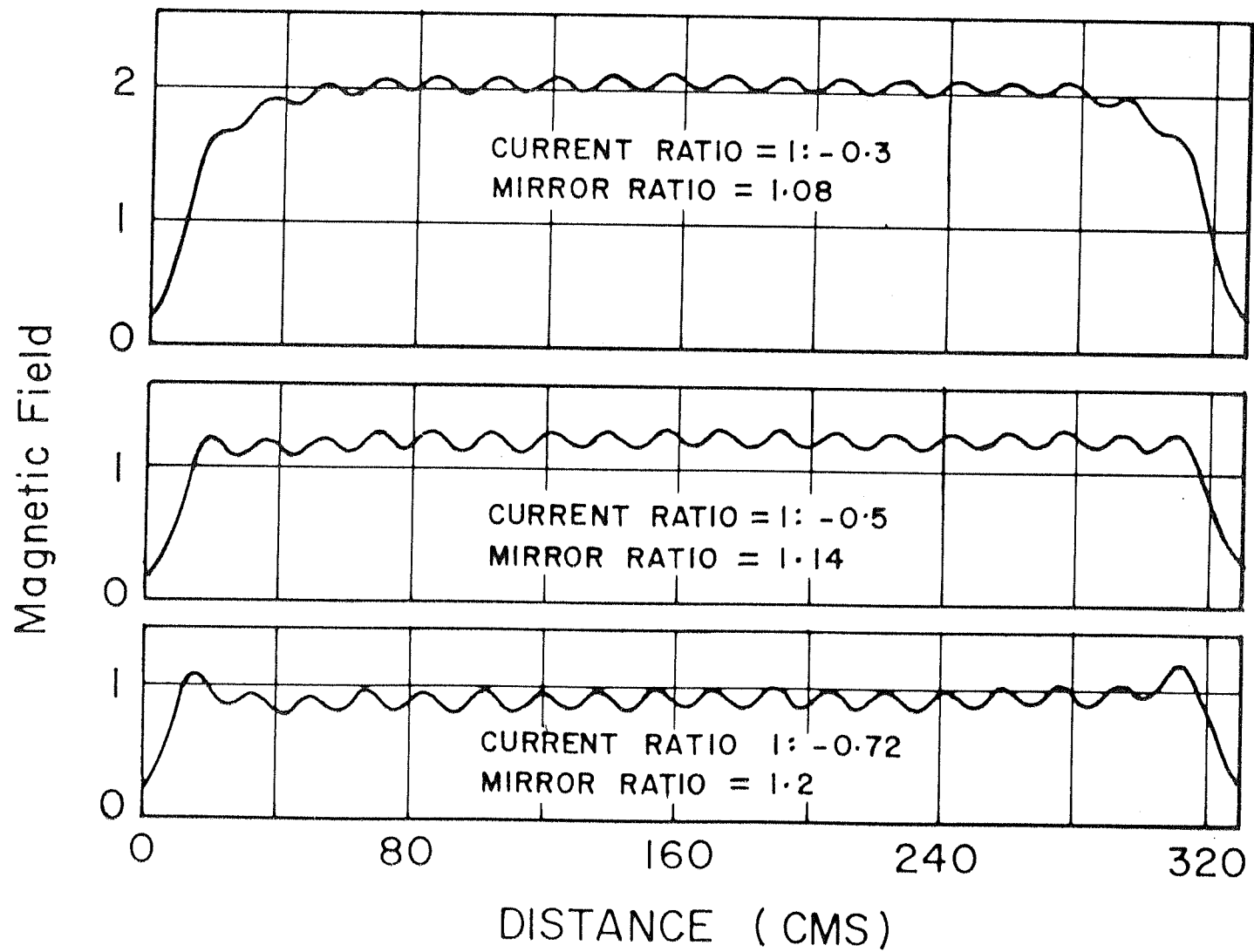


Fig.2.6 Experimental plots of magnetic field distribution

Using a digital gaussmeter, the actual values of the magnetic field were measured at different points along the axis in order to calibrate the above measurements.

For getting an experimental plot of the electron current, transmitted through the multimirror system, as a function of the amplitude of magnetic field the following procedure was adopted. The resistance box with the required value was connected in series with the even numbered coils. The autotransformers in the two DC power supplies, feeding the two sets of coils were rotated with two identical motors. By operating a single switch, the currents in the odd and even numbered coils were increased or decreased simultaneously, maintaining the same current ratio and hence the same mirror ratio in the system. The entire sweep of the magnetic field while obtaining a single plot does not exceed five seconds, thereby eliminating chances of any variations in the currents due to heating of the coils.

2.3. Electron Gun

An electrostatically focussed electron gun serves as the source of electrons in the experiment. The gun, having an unipotential einzel lens was designed to function in a range from 500-6000 eV. The gun is capable of giving a beam current upto 50μ A. The gun consists of a hollow cylindrical cathode with a 4 mm dia hole for the outlet of electrons. Electrons were emitted from a tungsten filament mounted inside the hollow cylinder. The lens was made of three cylindrical electrodes, placed in front of the cathode

aperture. A schematic of the electron gun drawn to scale is shown in fig. 2.7.

Two bridge rectified power supplies were used for the filament (0-10 V) and the cathode (0-10 KV). The rectified power supplies had a ripple factor not more than 0.3%. The potentials for the electrodes of the einzel lens were also obtained from the cathode power supply using a voltage divider.

In the initial stages, the gun was operated with the first and the third electrodes (V_1 and V_3) maintained at ground potential. The cathode and the filament inside it were maintained at the required negative potential. The potential on the second electrode, V_2 , was 0.4 times the cathode voltage.

With the help of a fluorescent screen the beam diameter was estimated to be about 0.4 cm at a distance of 10 cm away from the gun. By sweeping the analyzer grid voltage of the retarding potential analyzer, the spread in the parallel energy of a 1 KeV beam was found to be nearly 75 eV. The current (I) versus Voltage (V) characteristic and the $\delta I / \delta V$ versus V plots are shown in fig. 2.8.

After placing the gun in the magnetic field it was observed that in the presence of magnetic field the ratios of the voltages V_1, V_2 and V_3 did not affect the outgoing beam significantly and hence in all the experiments, the three electrodes of the lens were grounded and used as a collimator.

The injection angle of the beam and the radial position

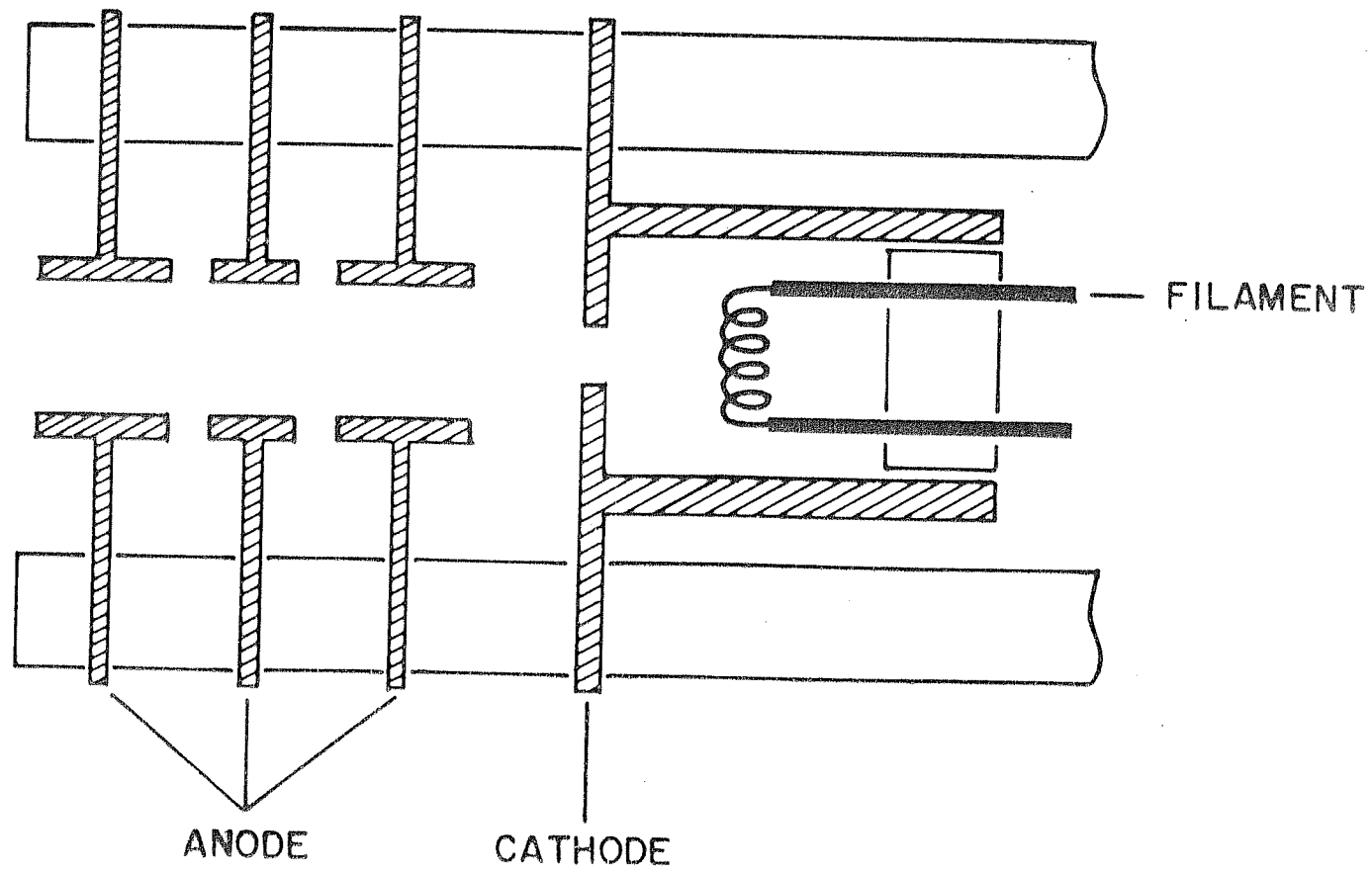


Fig.2.7 Schematic of the electron gun

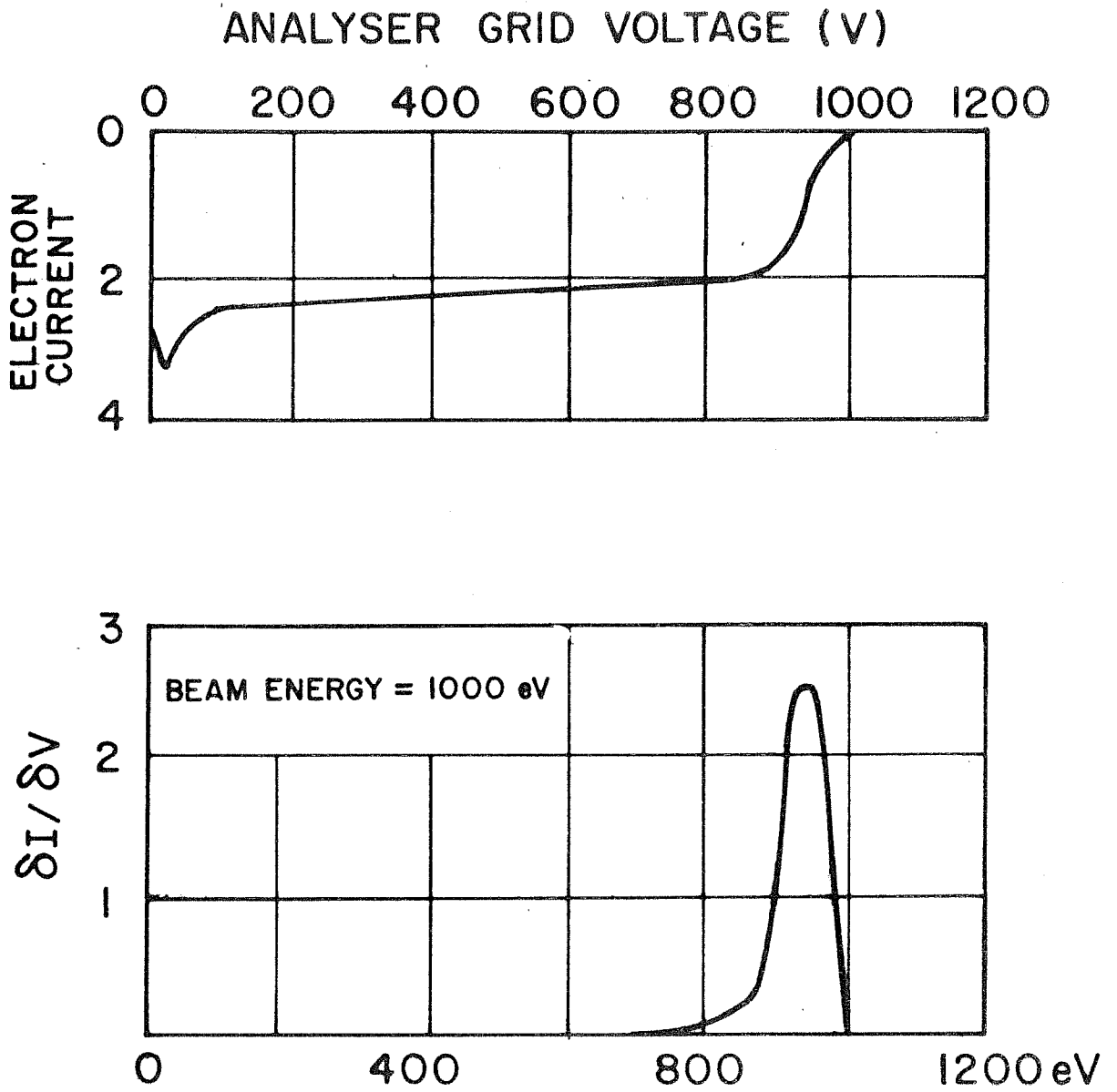


Fig.2.8 I-V characteristic and energy spectrum of electron beam

of the injection point were varied with the help of a system of gears without disturbing the vacuum in the system. Mechanical connections to the gears were taken out of the experimental chamber through Wilson feedthroughs for this purpose. The injection angle of the electron beam could be varied in the range from 0° to 90° with an accuracy of $\pm 2.5^{\circ}$. While carrying out experiments with the multimirror magnetic field configuration, the gun is situated in the region of the minimum of the first mirror. The electron gun has an overall length of 35 mm and the accelerating region itself is 8 mm in length. Therefore, with a mirror length = 17 cms., it was assumed that the magnetic field lines were parallel to the axis of the system over a region, covered by the length of the gun, and hence the angle made by the gun with the axis of the system is taken to be equal to the initial pitch angle and commonly referred to as injection angle in the text.

The electron gun could be moved radially upto a distance of 9 cms from the axis with an accuracy of better than 1 mm. The electron gun along with the mechanisms for the variation of its position is shown in the photograph in fig. 2.9.

2.4. Diagnostics

The main diagnostic element used in the experiment was a retarding potential analyzer. Since the experimental observations were to be carried out at different axial positions, for different beam energies, injection angles,

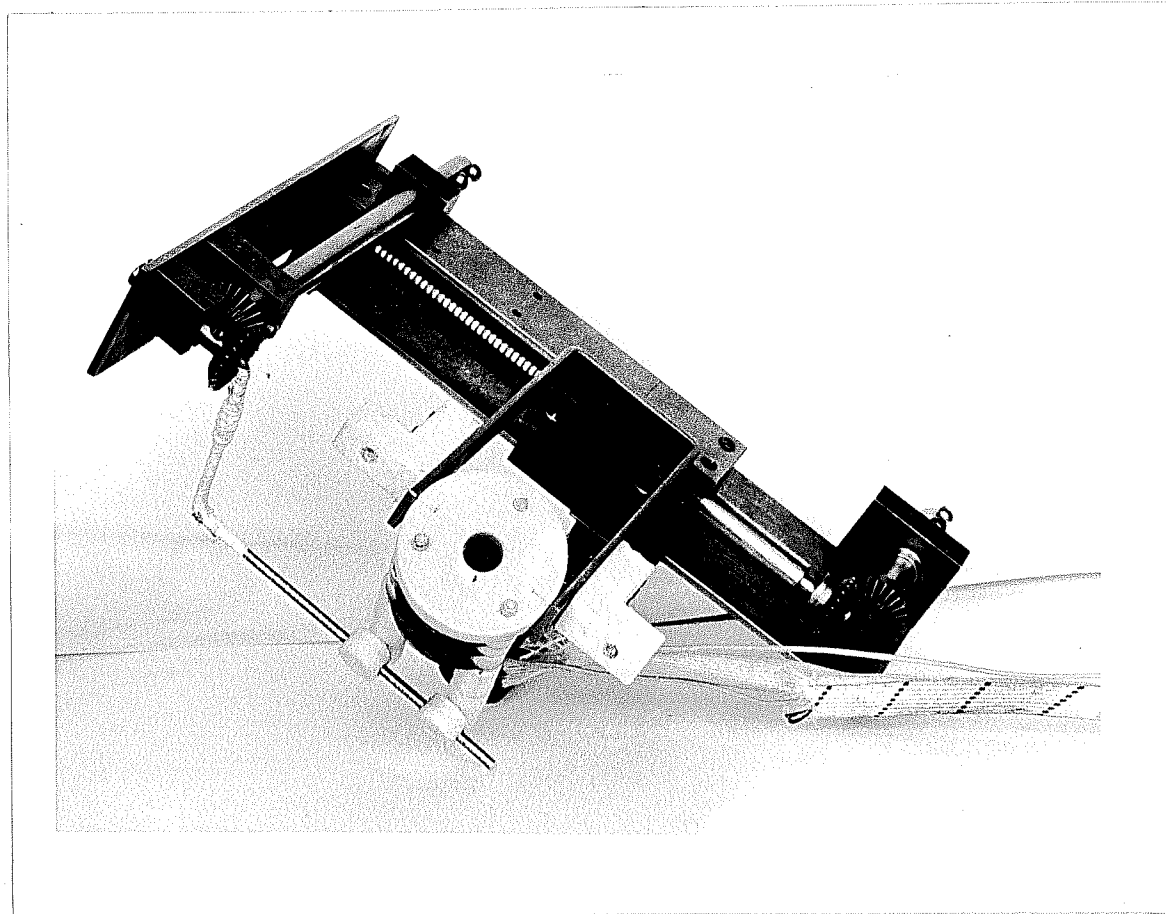


Fig.2.9 Electron gun with mechanism for varying injection angle and radial position

magnetic fields and mirror ratios, it becomes difficult to locate the position of the beam with the help of a small detector, especially since there are no radial ports. Hence experimental observations were made with the help of a single retarding potential analyzer large in comparison with the beam dimensions, whose position could be controlled from outside without disturbing the vacuum. The retarding potential analyzer is made of a stainless steel disc 22 cms in diameter and a stainless steel mesh placed in front of it. The mesh has 11x11 wires per sq. cm and wire diameter is equal to 0.018 cm. with a transparency of \approx 60% and is separated from the disc by 2 cms. using teflon spacers.

The analyzer is mounted on a trolley, movable along the length of the experimental chamber. A system of two spools rotated with the help of a common cylindrical rod from outside the experimental chamber, a system of pulleys at the two ends of the system and a stainless steel wire stretched along the entire length of the system enabled a smooth movement of the analyzer with the trolley. The analyzer could be moved in the region between 1st and 15th mirrors, i.e., a distance of nearly 250 cms with an accuracy of better than 2 cms. The electrical connections to the analyzer are made through electrical feedthroughs mounted on the end flange. A photograph of the retarding potential analyzer mounted on the trolley is shown in fig. 2.10.

For recording the current transmitted through the multimirror system, the analyzer grid was negatively biased to about 50 volts to eliminate secondary emissions. The



Fig.2.10 Retarding potential analyzer mounted on the trolley

electron current received by the detector was passed through a $0.5 \text{ M}\Omega$ resistor and the voltage across the resistor was fed to the X axis of an X-Y recorder. The block diagram of the circuit used to obtain transmitted current versus magnetic field plots is shown in fig. 2.11. The circuit used to obtain I vs. V plots for getting energy spectrum using the same detector is shown in block diagram in fig. 2.12.

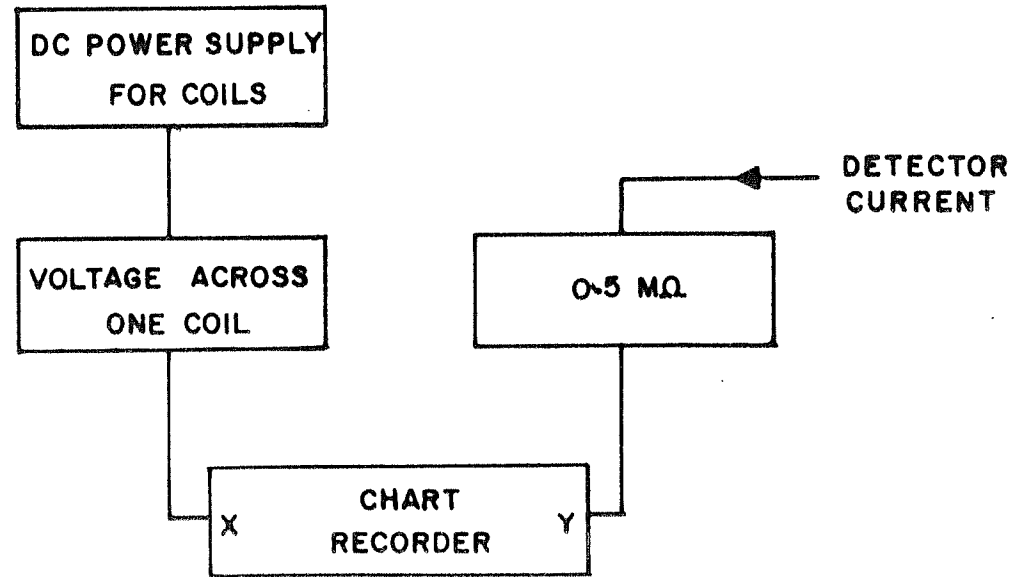


Fig. 2.11 Block diagram for obtaining transmitted electron current versus magnetic field plot

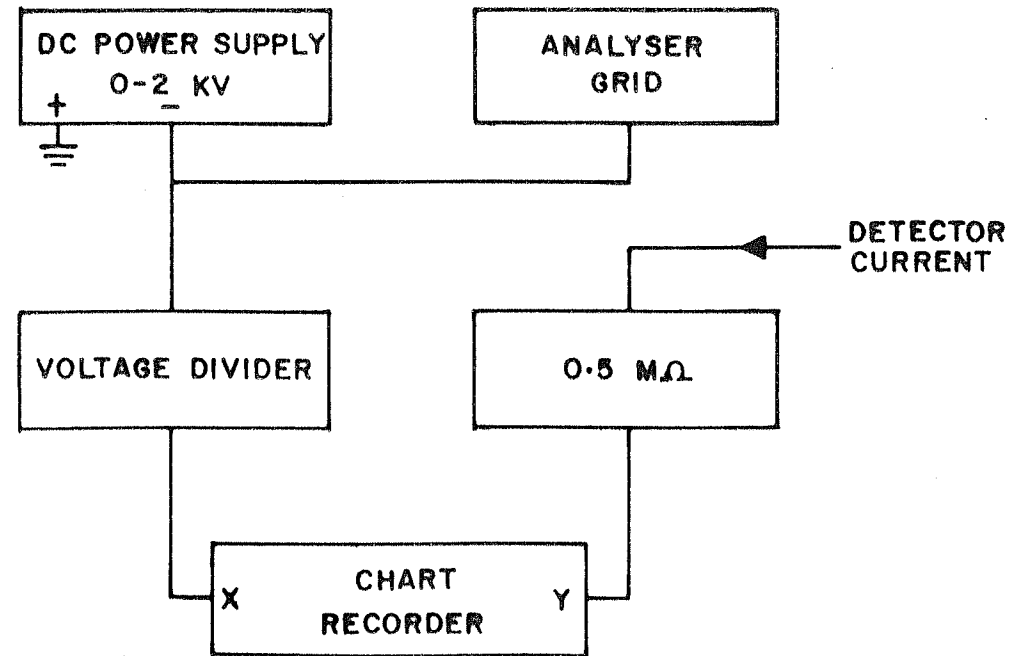


Fig.2.12 Block diagram for obtaining I-V characteristic with the retarding potential analyzer

Table 2.1

Dependence of the mirror ratio and magnetic field on
the ratio of currents in the even numbered to odd
numbered coils and mirror length.

Radius of each coil = 16 cms

Number of coils = 35

C_1 = current through odd numbered coils,

C_2 = current through even numbered coils,

L = Mirror length

C_2/C_1	L 17 cms	16 cms	15 cms	14 cms
-0.80	1.3713 (.0271)	1.252 (.0271)	1.1641 (.0286)	1.1019 (.0298)
-0.85	1.55 (.0214)	1.36 (.0216)	1.23	1.14 (.0228)
-0.90	1.985 (.0157)	1.616 (.0155)	1.381 (.0155)	1.214 (.0156)
-0.92	2.435 (.0134)	1.843 (.0130)	1.504 (.0128)	1.294 (.0129)
-0.94	3.559 (.0111)	2.327 (.0105)	1.738 (.0102)	1.417 (.0101)

The values shown in brackets, when multiplied by a factor $2\pi NI/10$ (where N is the number of turns in each coil and I is the current, in amperes, flowing in the odd numbered coils) give the value of maximum magnetic field (in gauss) in the central region of the multimirror system.

CHAPTER III

Experiments, Observations and Analysis

The experiment was proposed to be conducted in the following manner. A stream of monoenergetic electrons with the appropriate pitch angle would be injected into a multimirror system. The pitch angle of the electrons would be so chosen that the particles are initially inside the adiabatic loss cone of the mirrors. If the particles were adiabatic, they would be completely transmitted across the entire multimirror system. However, since the non-adiabatic effects always occur to some extent, some of the particles would get reflected from the system as a whole and the particles which do not get reflected by any of the mirrors would go out of the last mirror. Since it is difficult to introduce a diagnostics to register the reflected particles without disturbing the incident particles, the object of study would be the transmitted particles rather than the reflected particles. The transmitted current or the number of particles escaping the system would be measured with the help of a retarding potential analyzer. The energy of the

electron beam or magnetic field would be varied during the course of the experiment and whenever the necessary conditions for the occurrence of Bragg-like reflections are satisfied, the transmitted current would go through a minimum.

In the present experiment it was possible to study the dependence of the transmitted current on either the magnetic field or the beam energy, maintaining other parameters constant. In order to eliminate shot to shot variations it was decided to use the magnetic field as the variable retaining all other parameters including beam energy, injection angle and mirror ratio as constant during a particular experiment. As explained in the previous chapter the choice of magnetic field as the variable parameter enables us to obtain a plot of the transmitted current versus magnetic field within a few seconds, during which one can be sure about the constancy of all other parameters.

3.1. Dependence of Transmitted Electron Current on the Magnetic Field

In order to carry out a systematic study of the behaviour of charged particles in the multiple mirror configuration, the experiments were carried out with different mirror ratios. The transmitted current versus magnetic field plots were obtained in each case in a manner as shown in fig. 2.11.

A nearly homogeneous magnetic field (mirror ratio $<$

1.005) along the length of the multimirror system was obtained by passing currents of equal amount and in the same direction in both sets of coils. A plot of the electron current registered by the retarding potential analyzer, placed in the region of the 9th mirror, as a function of the magnetic field, maintaining the other parameters i.e., injection angle ($= 32^\circ$), beam energy ($= 800$ eV) constant, is shown as a continuous curve in fig. 3.1. The shape of the transmitted electron current versus magnetic field plot is explained by the fact that the gun is positioned with its axis subtending an angle, equal to 32° , with the axis of the chamber. At zero magnetic field the beam coming out of the gun travels straight and hits the wall of the chamber in the region of the first mirror. With an increase in magnetic field the $V \times B$ force bends the trajectory of the particle. Since there is a small dispersion in the beam energy, the particles with the least perpendicular energy enter first into the multimirror system. With a further increase in the field the trajectories of more and more electrons are bent and transmitted into the multimirror system. After the current hits a saturation point a further increase in the magnetic field reduces the total number of electrons coming out of the gun, since the Larmor radius of the electrons decreases to such an extent that they hit the walls of the three cylindrical electrodes, placed in front of the cathode. Thus at high values of magnetic fields the transmitted current again becomes zero. Experiments carried out with different injection angles and beam energies show that at

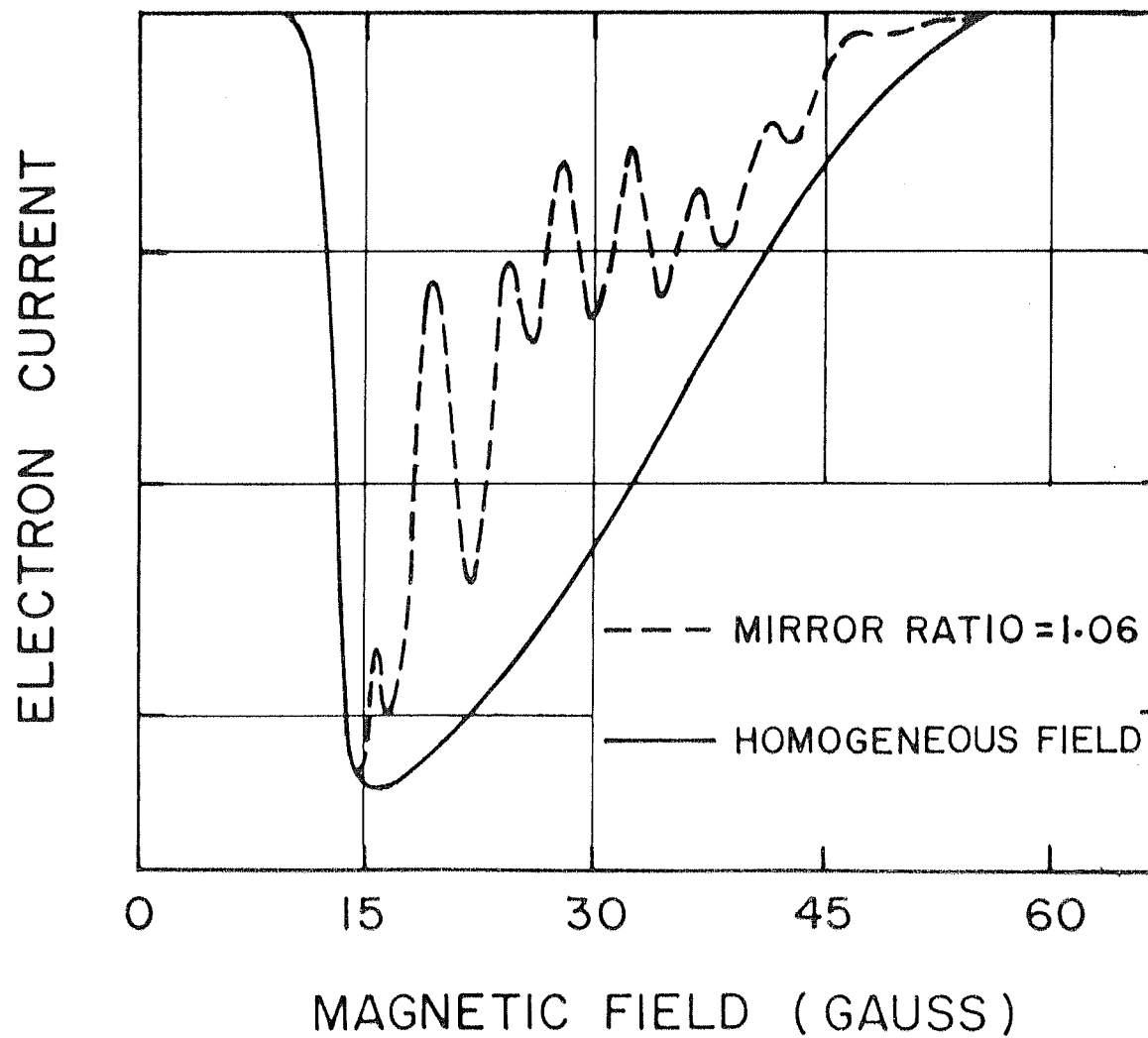


Fig.3.1 Transmitted electron current as a function of magnetic field, recorded 10 mirrors away from the electron gun, Beam energy = 800 eV, injection angle = 32° .

low injection angles the transmitted current starts appearing at lower values and disappears at higher values of magnetic field compared to the corresponding values for higher injection angle. Similar behaviour is observed with a change in beam energies, the transmitted current plots are wider for lower beam energies in comparison with those corresponding to higher energies. A fast rise and slow fall of the transmitted current could probably be explained by the fact that the Larmor radius is inversely proportional to the value of magnetic field and hence the dependence of Larmor radius with the magnetic field is a hyperbolic function.

A plot of the transmitted electron current versus magnetic field, registered by the retarding potential analyzer, with the grid biased to -475V and placed in the 9th mirror region maintaining injection angle $= 32^\circ$ and beam energy $= 800\text{ eV}$ constant and a mirror ratio $= 1.06$ is also shown in fig. 3.1 by a dotted curve. A comparison of these two curves clearly shows that the passage of the electron beam through the 8 mirrors has caused dips in the transmitted current at discrete values of magnetic field. Similar results were obtained for other beam energies, injection angles and mirror ratios.

In fig. 3.2, we have shown four plots of the transmitted current versus magnetic field obtained in the cases of different voltages applied to the analyzer grid. The experimental parameters were; injection angle $= 32^\circ$, beam energy $= 1000\text{ eV}$ and mirror ratio $= 1.06$. It is clear from

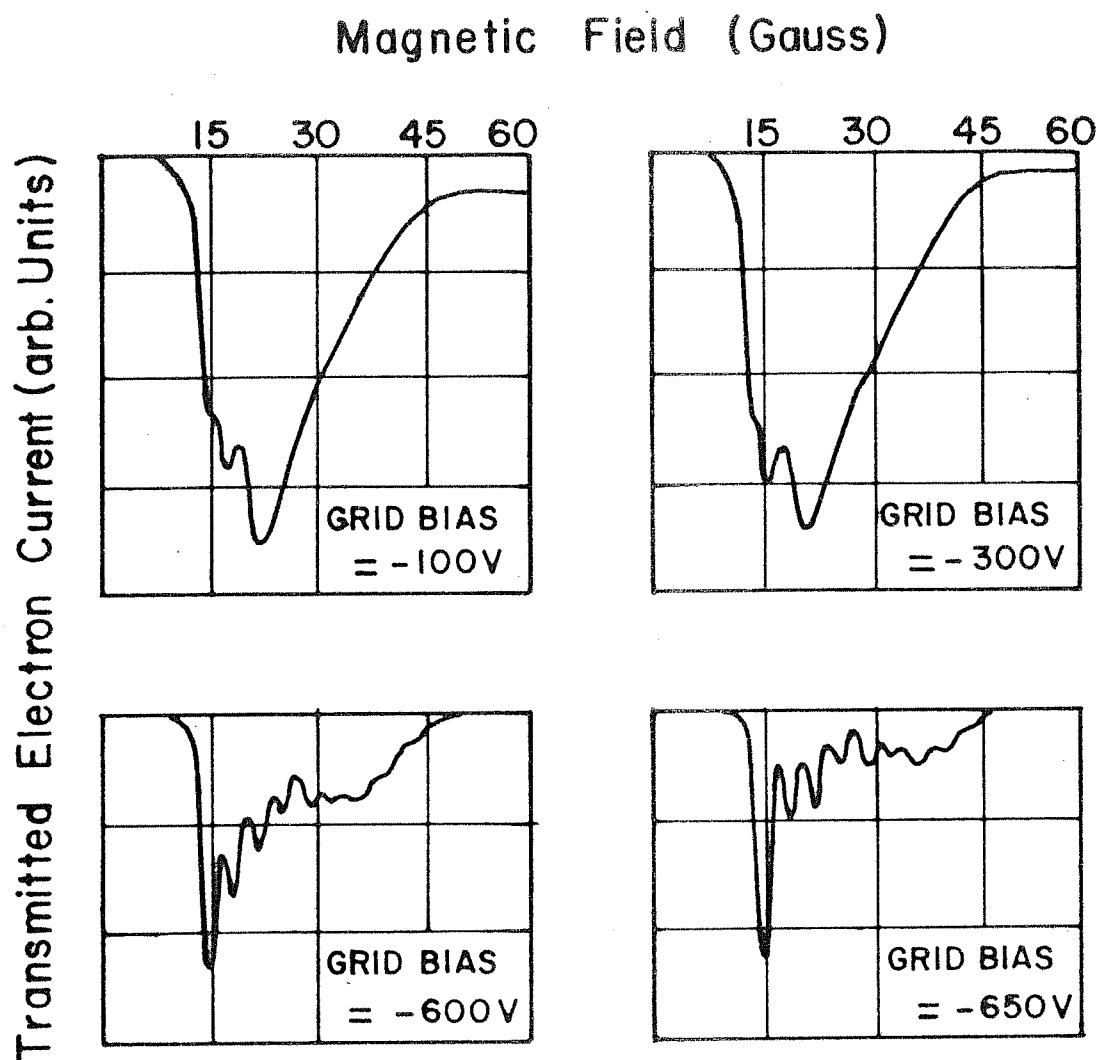


Fig. 3.2 Transmitted electron current versus magnetic field plots recorded 13 mirrors away from the gun at different analyser grid voltages. Beam energy = 1000 eV, injection angle = 32° and mirror ratio = 1.06.

these plots that when the grid voltage is low compared to the parallel component of the beam energy, the plot contains only two or three dips. An increase in the bias voltage does not affect the behaviour significantly till it becomes comparable to the parallel energy of the beam, when an increase in the grid voltage reveals several other dips in the plot. This phenomenon can probably be explained in the following manner. The dips in the transmitted current plot, when the grid voltage is equal to zero, correspond to the resonance interactions, which have resulted in the reflection of particles, before they reach the analyser. The same is the nature of the dips, which remain unchanged till the grid voltage becomes comparable to the parallel energy of the beam. After this, any further increase in the grid voltage leads to a reduction in the transmitted current, simultaneously revealing several more dips in the transmitted current plot. These dips are associated with the electrons, whose parallel energy has been partially converted into the perpendicular energy because of the resonances at the corresponding values of the magnetic field. It should be noted that, unlike the reflection of electrons causing dips at zero grid voltage, these electrons have not transferred all their parallel energy to the perpendicular energy. It may further be pointed out here that the mirror ratio 1.06 corresponds to a loss cone angle equal to 85° and hence the injection ($\theta = 32^\circ$) in our case is very much inside the loss cone. The orders and modes, which have the highest growth rates, may result in

reflection of the particles and the other orders and modes would result in just decreasing the parallel energy. An injection at an angle lying just inside the loss cone, if achieved, could probably lead to dips, corresponding to reflections and not just a decrease in the parallel energy.

3.2. Dependence of the Position of dips on the Beam Energy

After prima-facie establishing that the passage of an electron beam through a periodic magnetic field leads to the appearance of several minima in the transmitted current versus magnetic field plot, as would be expected from the predictions of the theory, it becomes necessary to carry out certain quantitative analysis to verify the theoretical predictions. One such dependence, which could be easily checked is the dependence of the position of a dip corresponding to a particular mode and order as a function of energy. As is seen in the relations (Eq. 1.35), (Eq. 1.37) and (Eq. 1.51) from Chapter I, the dependence of the position of a dip on the square root of beam energy is linear. Figs. 3.3 a,b show the results of two experiments, where the detector was positioned in the region of the third mirror, and the dependence of the positions of the first and second dips are plotted against the square root of beam energy. Fig. 3.3 a is obtained for the injection angle = 42° and fig. 3.3b for injection angle = 12° . The theoretically expected dependences according to the equations (1.37) and (1.51) are also plotted on the same figures corresponding to $2\Omega = 2\omega_t$ and $2\Omega = 3\omega_t$. Many more

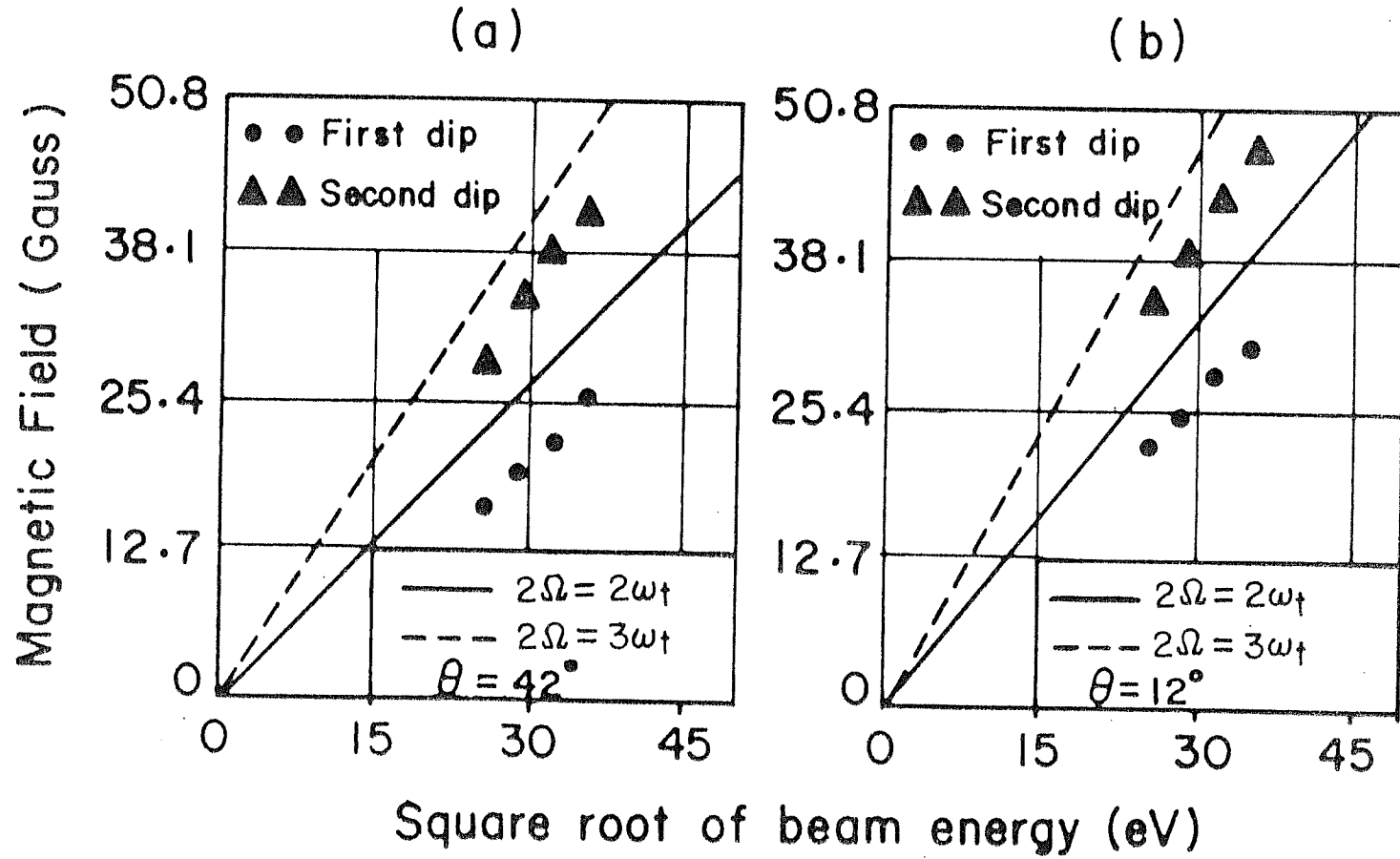


Fig.3.3 Dependence of the position of the dips in transmitted current on square root of electron beam energy in the third mirror region. Mirror ratio = 1.06.

such dependences, obtained for various other initial pitch angles and mirror ratios, have shown that the dependence is linear and close to the theoretically predicted line corresponding to equations (1.37) and (1.51). It is important to note here that the distance between the adjacent dips in the transmitted current, when plotted as a function of square root of beam energy also gives a linear dependence, further confirming the theoretical prediction. The deviations of the experimental values from the theoretical lines corresponding to different orders and modes of equations (1.37) and (1.51) as seen in figs. 3.3a, b, could probably be attributed to an error in the estimation of injection angle θ . The possibility of an error in the determination of θ is discussed in Chapter IV. A slight increase in the value of θ would result in a reduction of the slopes of the theoretical lines and bring them closer to the experimental values.

3.3. Dependence of the Position of Dips on the Injection Angle

A further verification of the theory could be carried out by checking the dependence of the positions of the dips on the injection angle. For this purpose, several transmitted current versus magnetic field plots were obtained placing the retarding potential analyzer in the region of the third mirror, and repeating the experiments for different values of injection angle. The position of the first and second dips as a function of injection angle θ was plotted. Such

plots were obtained for different values of the beam energy. Two typical cases for beam energies equal to 1250 eV and 625 eV are shown in fig. 3.4 a,b. In the same figures are shown the theoretically predicted dependences which follow from the equations (1.37) and (1.51), for beam energies 1250 eV and 625 eV. The dependence of the positions of the first dip is found to be situated close to the theoretical curve corresponding to $2\Omega = 2\omega_t$ and that of second dip is close to the theoretical curve corresponding to $2\Omega = 3\omega_t$. At low values of injection angle, when the transmitted current signal covers a wider range of magnetic field one could also notice a new dip at a lower value of magnetic field, the position of which is close to the theoretical curve for $2\Omega = \omega_t$. We could not obtain the dependence of this dip on the injection angle because the transmitted current becomes very small and ultimately zero at this value of the magnetic field with an increase in θ .

3.4. Measurements Carried Out at Different Axial Positions

As we have seen earlier in fig. 3.1, the transmission of the electron beam through the multimirror system leads to the appearance of several dips in transmitted current. In order to understand the genesis of the number of dips observed, a series of such plots were obtained at more than 60 different positions along the multimirror system. In each case the analyzer grid was maintained at a voltage slightly less than the initial parallel energy of the beam. In figs. 3.5 a, b, c are shown 30 such plots, obtained at various

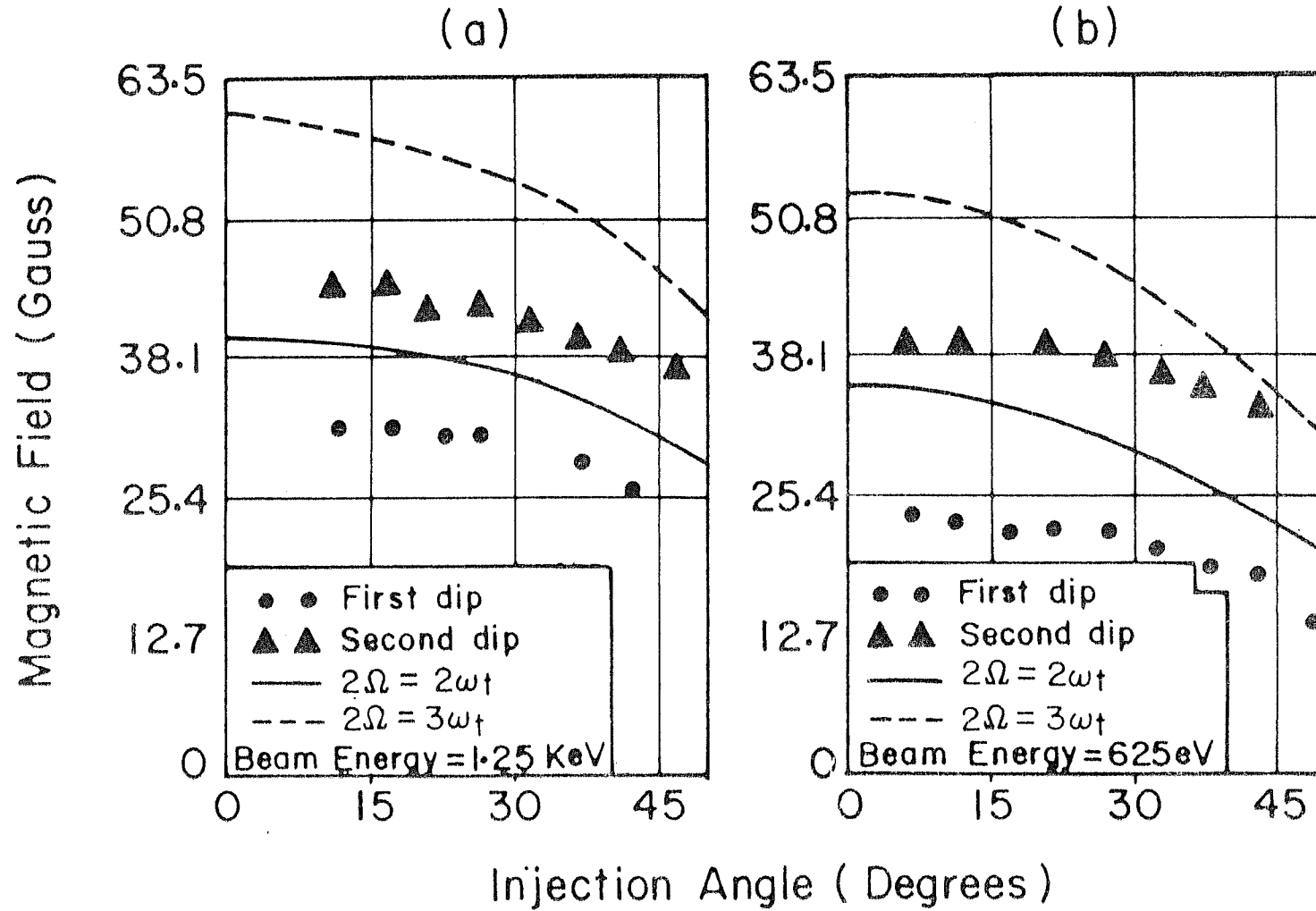


Fig.3.4 Dependence of the position of the dips in transmitted current on injection angle θ in the third mirror region. Mirror ratio = 1.06.

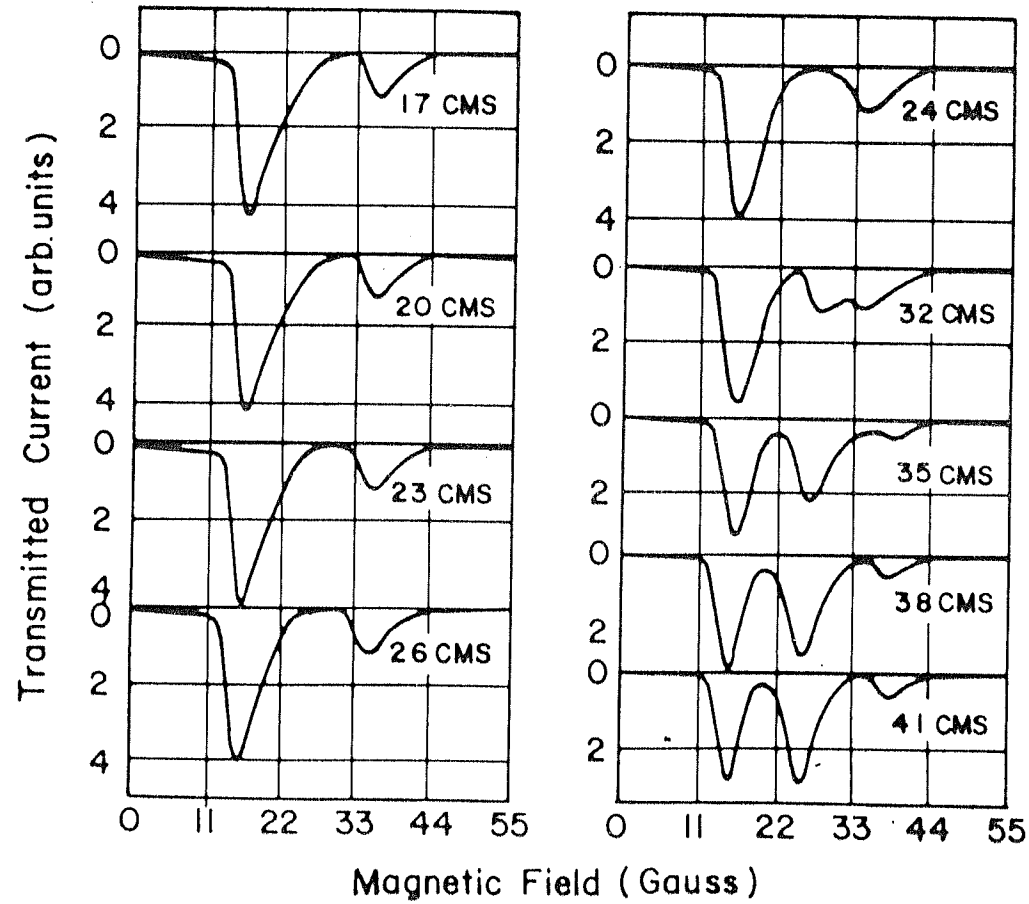


Fig.3.5(a) Transmitted electron current as a function of magnetic field at different axial positions. Beam energy = 800 eV, injection angle = 37° and mirror ratio = 1.06.

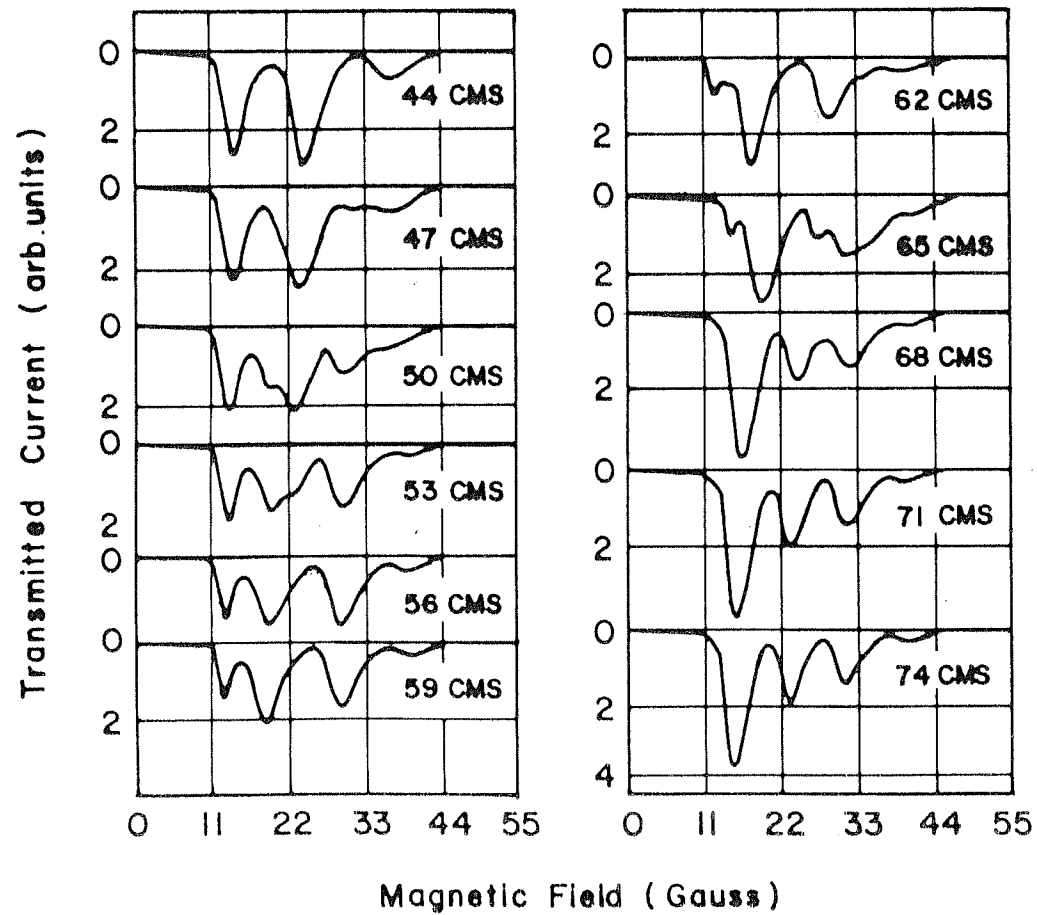


Fig.3.5(b) Transmitted electron current as a function of magnetic field at different axial positions. Beam energy = 800 eV, injection angle = 37° and mirror ratio = 1.06.

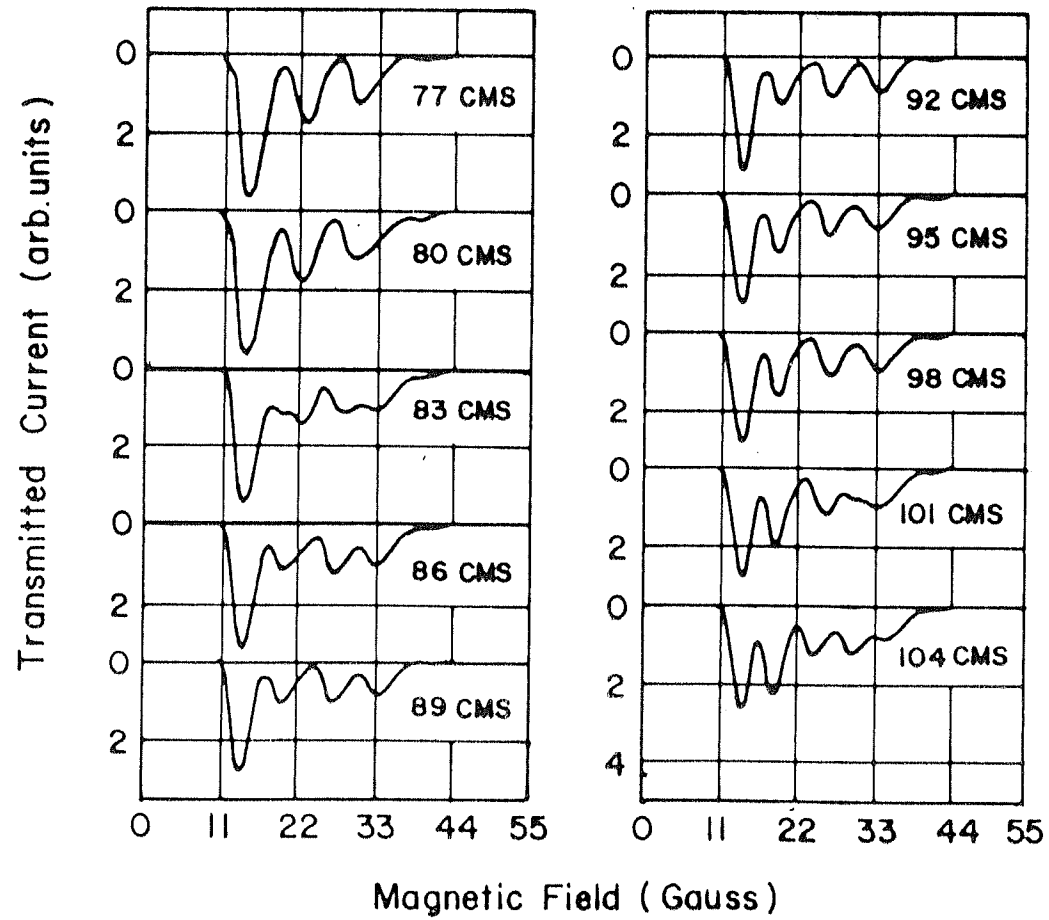


Fig.3.5(c) Transmitted electron current as a function of magnetic field at different axial positions. Beam energy = 800 eV, injection angle = 37° and mirror ratio = 1.06.

positions of the analyzer, starting from the region of the second mirror and ending in the region of seventh mirror. Each consecutive plot was obtained after moving the analyzer by a distance of 3 cms. A typical observation made during these experiments is that as the electron beam travels through more and more mirrors the number of dips, observed in the plot, increases from one, two, three and so on. In this manner we have observed a maximum of 8 dips, when the analyzer is moved to distances more than 8 mirrors away from the gun. From the particular illustration shown in figs. 3.5 a, b, c, it may appear that after passing through an additional mirror a new dip appears. However, other experiments carried out with lower mirror ratios show that a new dip does not necessarily appear after the passage of every mirror. Another point to be noted is that in the experiments carried out by us, the number of dips was found to be never greater than the number of mirrors travelled by the electron beam. We have attempted to give an explanation for the above phenomenon in Chapter IV. We have shown that the relation $\ell \Omega = n \omega_c$, corresponding to the resonance interaction taking place when the electron completes n cyclotron rotations during the passage through ℓ spatial periods of the magnetic field, should give progressively increasing number of dips in the transmitted current plot with an increase in the number of mirrors travelled by the beam.

A close observation of the plots in figs. 3.5a, b, c shows that after the appearance of a particular dip in the

plot, a movement of the detector away from the gun leads to the shifting of the dip towards lower values of the magnetic field. After the dip has thus moved to the left, a further movement of the detector away from the gun leads to the appearance of a new dip at a higher value of magnetic field. This observation is illustrated in fig. 3.6.

It is pertinent to note here that the description of the shifting of the dip towards lower magnetic field values as shown in fig. 3.6 is just a simplified picture of the experimental observations. Close to the gun the dip in the transmitted current is wide and as the detector is moved away more and more dips appear, which are narrower than the dips, appearing close to the gun. Further in the plots reproduced in figs. 3.5a,b,c we notice that as the detector is moved away at times a kink appears first, disappears later giving rise to a new dip. Hence the phenomenon is much more complicated than the description, which does not take into account all these complexities. The above phenomenon of shifting of the dips towards lower values of magnetic field as the analyzer is moved away from the gun could probably be explained by the fact that as the beam travels through the multimirror system, the parallel energy gets converted into perpendicular energy because of the resonant interaction. A decrease in the parallel velocity would in turn lead to a reduced ω_t and hence a resonance with a particular order and mode would now take place at a lower value of the magnetic field.

Energy analysis of the electrons reaching the analyzer,

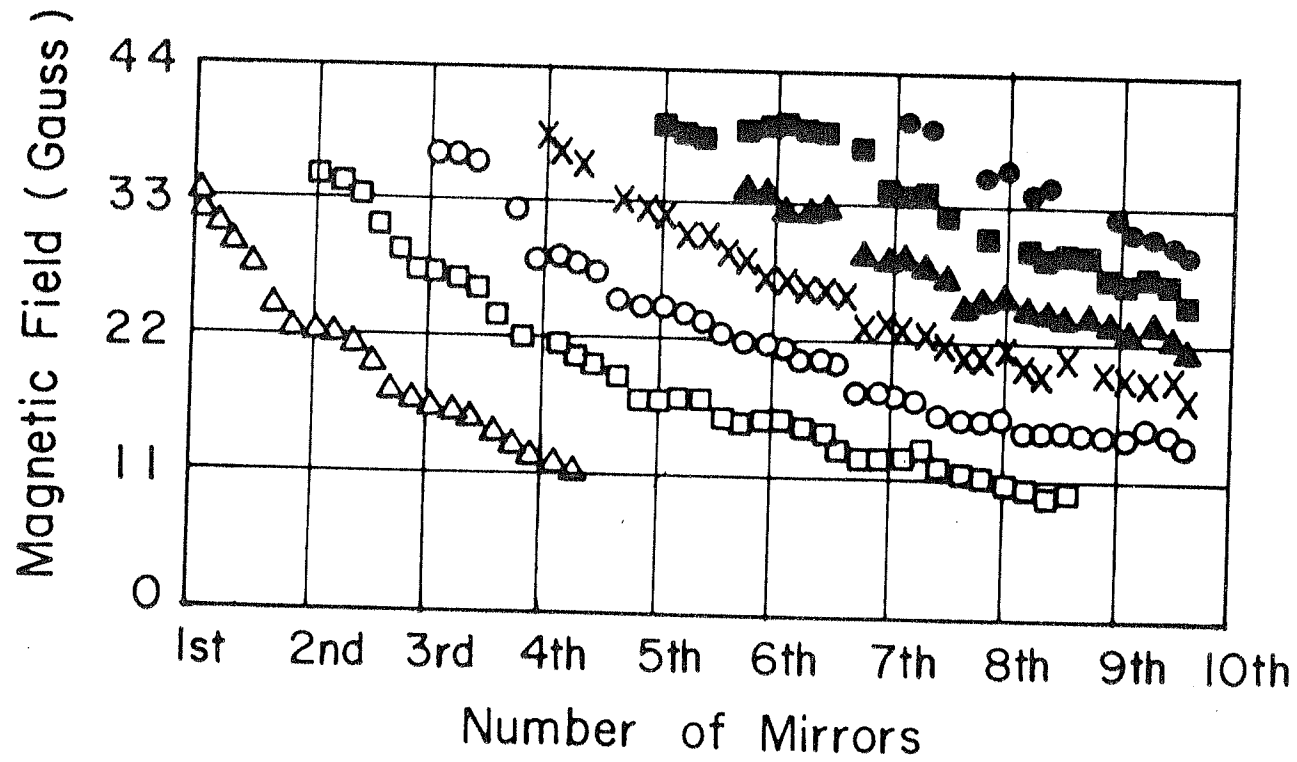


Fig.3.6 Position of dips as a function of distance from the electron gun.
 Beam energy = 800 eV, injection angle = 37° and mirror ratio = 1.06.

for the magnetic field corresponding to the 1st dip was carried out at different points along the axis of the system. In fig. 3.7, the energy spectrum obtained at different distances from the electron gun is reproduced. Fig. 3.8, which is the observed dependence of peak parallel energy on the distance from the electron gun, shows that the parallel energy of the beam at the magnetic field corresponding to the dip shows a decreasing trend as the electrons travel deeper into the multimirror system. This result is in agreement with the observation of Fedorchenko et al.¹⁸ who have shown a sharp increase in the perpendicular energy of the electrons as they travel through an increasing number of mirrors (Fig. 1.3b). The slower drop in the parallel energy in our observations at fig. 3.7 may be due to the lower mirror ratio 1.06 in our case as compared to the case with the ratio 1.25 in fig. 1.3b.

3.5. Energy Analysis at the Position of Dips and Peaks of the Transmitted Current Plot

Experiments were carried out to measure the parallel energy of the beam after it passes through the multimirror system at different values of magnetic field. For this purpose a typical case, as shown in fig. 3.11, was chosen. This plot was obtained by placing the analyzer 10 mirrors away from the gun. The beam energy was equal to 600 eV, mirror ratio was equal to 1.06 and the injection angle was 37° . The currents in the field coils were adjusted each time

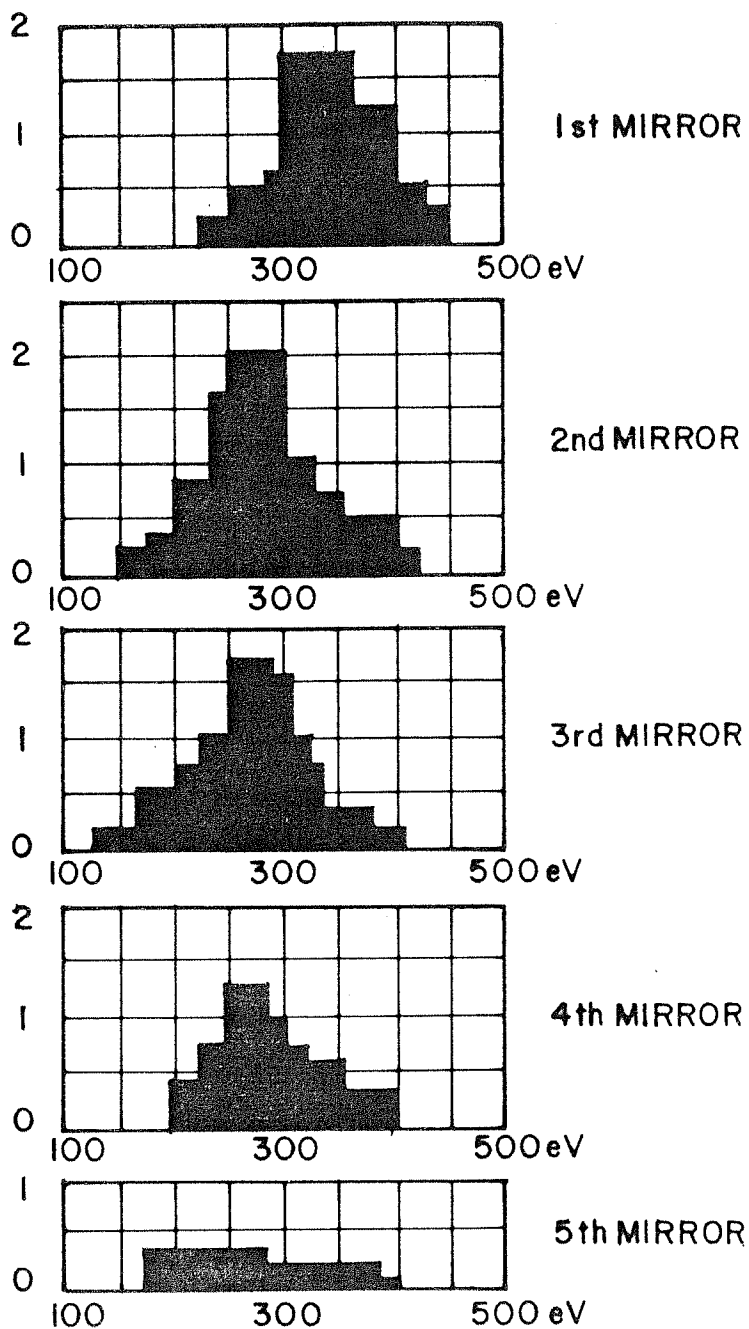


Fig. 3.7 Spectrum of parallel energy of electrons at the first dip at different distances from the gun. Beam energy = 600 eV, injection angle = 37° and mirror ratio = 1.06.

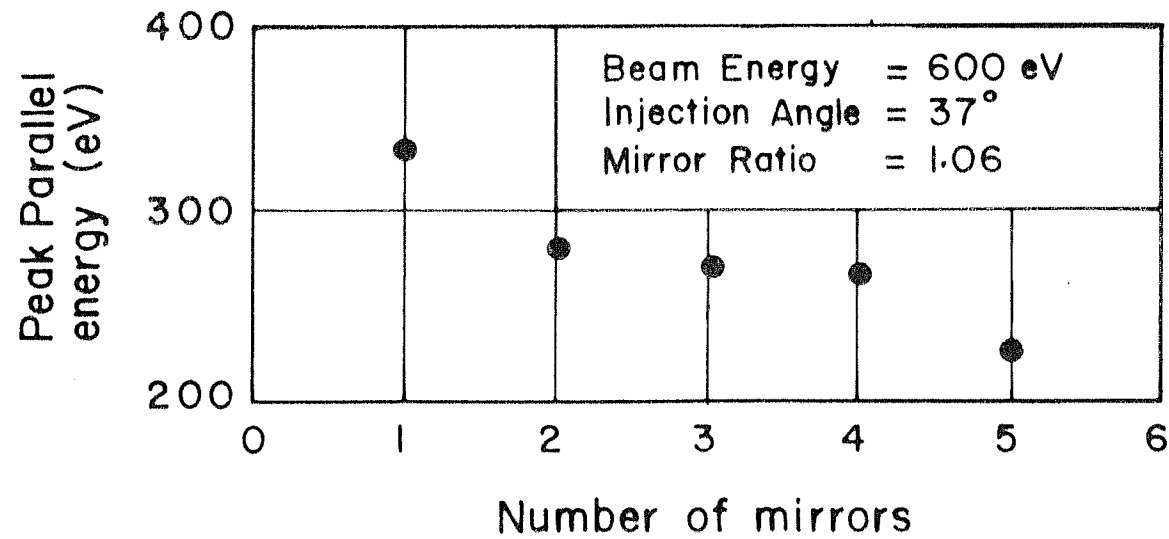


Fig.3.8 Parallel energy of electrons at the first dip as a function of distance from the electron gun. Beam energy = 600 eV, injection angle = 37° and mirror ratio = 1.06.

to produce different values of magnetic field covered in this plot. In every case the voltage on the analyzer grid was swept from 0-600 V and from these I vs. V plots the energy spectra were obtained. The energy spectra obtained at different values of magnetic field are shown in figs. 3.9a, b. An analysis of these spectra shows that in the neighbourhood of the values of magnetic field, where the dips occur, the spectrum of parallel energy of electrons gets broadened and shifts towards lower values of energy. Further, the energy spectra obtained at 27 different values of magnetic field consistently show that at values corresponding to dips there is a decrease in parallel energy and at values corresponding to peaks, the spectra become sharp and narrow and shift to values, higher than the initial parallel energy of the beam. The peak energy values obtained from these spectra are plotted against the value of the magnetic field in fig. 3.10. A comparison of this curve with the transmitted current plot at fig. 3.11 shows that every dip corresponds to a minimum in the plot at fig. 3.10. Further, a comparison of the values of cyclotron frequency at the point of occurrence of the dips with the transit frequency ω_t shows that the different dips in the transmitted current plot of fig. 3.11, correspond to $4\Omega = 2\omega_t$, $4\Omega = 3\omega_t$, $4\Omega = 4\omega_t$, $4\Omega = 5\omega_t$ and $4\Omega = 6\omega_t$. Similar analyses were also carried out with the transmitted current plots, obtained at different distances from the electron gun along the length of the system. The correspondence of the observed dips in these cases can be

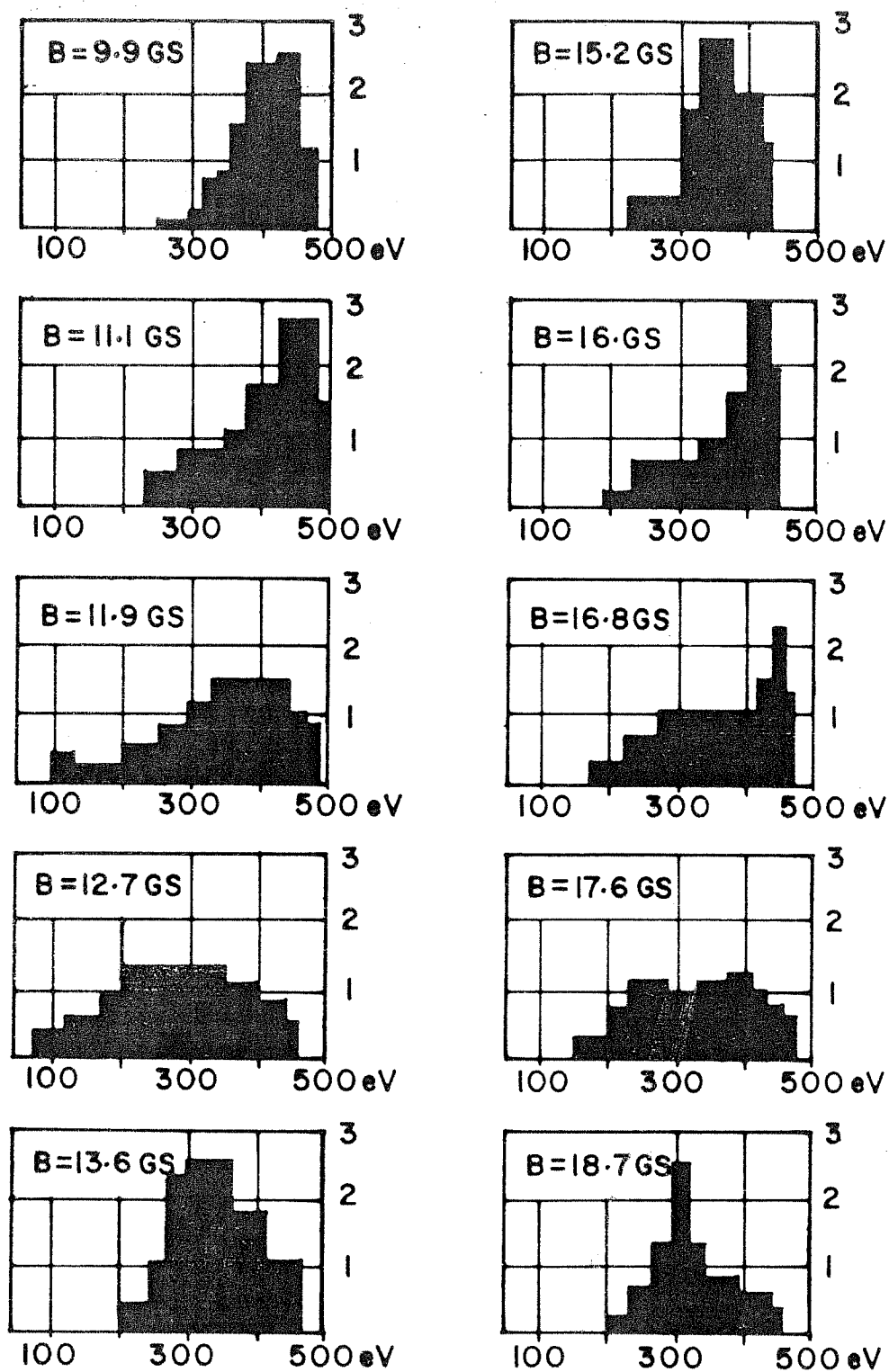


Fig.3.9(a) Spectrum of parallel energy at different magnetic fields. Beam energy = 600 eV, injection angle = 37° and mirror ratio = 1.06.

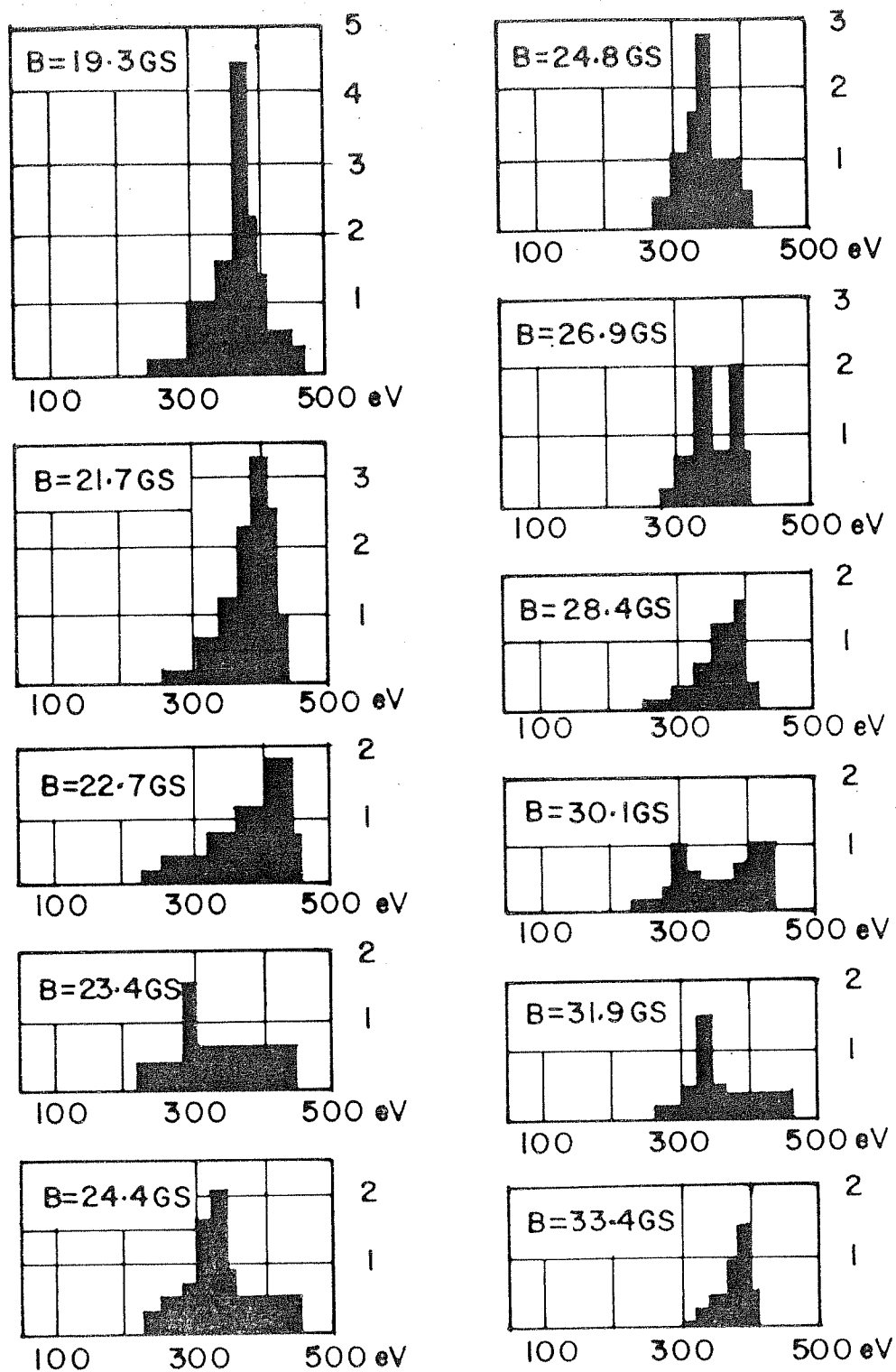


Fig. 3.9(b) Spectrum of parallel energy at different magnetic fields. Beam energy = 600 eV, injection angle = 37° and mirror ratio = 1.06.

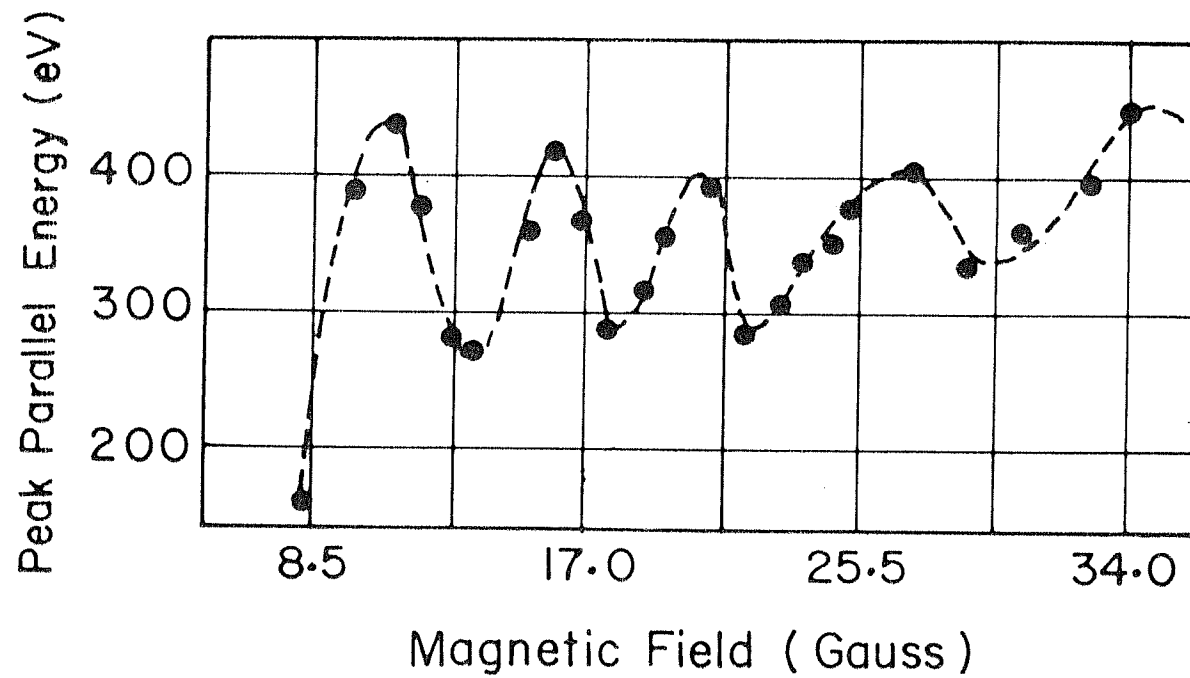


Fig.3.10 Peak of parallel energy as a function of magnetic field. Beam energy = 600 eV, injection angle = 37° and mirror ratio = 1.06.

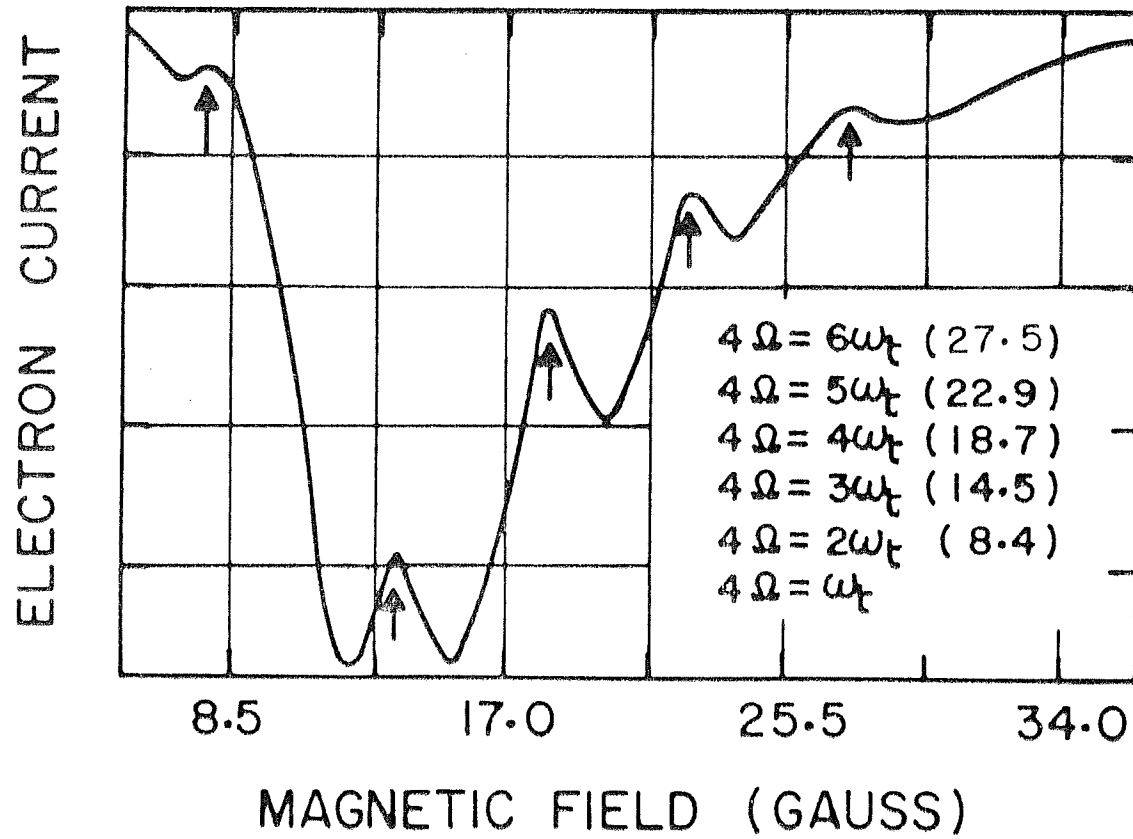


Fig.3.11 Transmitted electron current versus magnetic field, recorded 10 mirrors away from the electron gun, showing various orders and modes of the relation $4\Omega = n\omega_t$. Beam energy = 600 eV, injection angle = 37° and mirror ratio = 1.06.

tabulated as under:

Distance from Electron Gun	Observed Relations
1 mirror	$\Omega = \omega_t$
2 mirrors	$2\Omega = 2\omega_t$ and $2\Omega = 3\omega_t$
4 mirrors	$3\Omega = 3\omega_t$, $3\Omega = 4\omega_t$ and $3\Omega = 5\omega_t$
7 mirrors	$4\Omega = 3\omega_t$, $4\Omega = 4\omega_t$, $4\Omega = 5\omega_t$, $4\Omega = 6\omega_t$ and $4\Omega = 7\omega_t$
10 mirrors	$4\Omega = 2\omega_t$, $4\Omega = 3\omega_t$, $4\Omega = 4\omega_t$, $4\Omega = 5\omega_t$ and $4\Omega = 6\omega_t$

CHAPTER IV

Discussion, Conclusions and Scope for Future Work

As we have already mentioned in the first chapter, amongst the investigations studying the passage of an electron beam through a spatially periodic magnetic field, there are mainly two different approaches by which the interaction is being looked at.

One of the approaches has been to look at the interaction as a case of parametric resonance. Parametric resonances are known to occur in the case of a particle interacting with time varying magnetic field, where the particle gains energy at certain resonance conditions^{25,26}. In the case of a spatially periodic magnetic field there is no external source of energy and the total energy of the particle cannot increase under resonance conditions. Hence the growth of perpendicular energy can take place only at the expense of parallel energy. The Mathieu's equation, describing the Larmor rotation (equation (1.40)), has unstable solutions for the Larmor radius at certain resonance conditions, the first of them being $\Omega = \omega_t$.

The other approach described in section (1.2)⁹ is based on the conclusions arrived at in a study of the behaviour of ensemble of particles in inhomogeneous magnetic fields. It has been observed (equation (1.30)) that the motion of charged particles in an inhomogeneous magnetic field is described by an equation, analogous to Schroedinger's equation in quantum mechanics. In this equation the parameter μ/q plays the role of \hbar . One of the important consequences of this approach is the prediction of the existence of multiple life times in the decay of charged particles, trapped in a magnetic mirror, for the verification of which experiments were carried out by D. Bora et al¹⁰. The experiments have shown that there are at least two life times in the decay of particles and these are found to vary with the experimental parameters in accordance with the predictions of the theory⁸.

The other consequence of the same approach is the occurrence of Bragg-like reflections. In the quantum analogue, for observing Bragg reflections of electrons, one requires periodic reflecting planes spaced several angstroms apart from each other and hence the periodic potentials of a crystal lattice happen to be the suitable structure for obtaining Bragg reflections. In the case of equations (1.30), with μ/q replacing \hbar , for commonly used experimental parameters, the distance between reflecting planes can be as high as 10 to 20 cms for observation of one-dimensional interference-like effects. In section (1.3), we have studied the possibility of observation of these effects in a

multimirror machine, a number of magnetic mirrors joined end to end, and as necessary conditions for the occurrence of the same, two different relations, namely,

$$4D = \frac{n}{q} \frac{2\pi}{\Omega} \sqrt{\frac{2E}{m}} \sin \theta \tan \theta \quad (1.35)$$

for the ideal case when there is no dispersion in μ and

$$2D = \frac{n}{q} \frac{2\pi}{\Omega} \sqrt{\frac{2E}{m}} \cos \theta \quad (1.37)$$

for the case when the initial μ contains a dispersion, were obtained.

Apart from the differences in the approach, we notice a difference in the predictions too. The existing literature considering the interaction as a parametric resonance predicts effects at

$$\Omega = n\omega_t \quad (n=1, 2, 3, \dots)$$

and in experiments¹⁸ and numerical simulations²¹ the authors have observed only one resonance i.e. $\Omega = \omega_t$ except in the experiments of R. Demirkhanov et al²³, where the authors have reported about the observation of a second resonance at $2\Omega = \omega_t$, in a spatially helical magnetic field structure. For the occurrence of Bragg-like reflections in the case of an electron beam with a dispersion in initial μ equation (1.36) gives

$$2q\Omega = n\omega_t$$

Such being the theoretical predictions arising out of

the different approaches, we set about carrying out experiments to verify the occurrences of the various resonances.

We are still not very clear as to why the authors of earlier investigations^{18, 20, 24} could not observe the different orders and modes except the interaction corresponding to $\Omega = \omega_t$, inspite of the fact that the modulation factors were very high, compared to our experimental parameters. In our experience, even the preliminary experimental shots showed several dips in the transmitted current versus magnetic field plot and the dependences of the position of these dips on the beam energy indicated that these dips correspond to the different modes and orders of the relation $l \Omega = n \omega_t$ (equation 1.51). One major difference in our experiments compared to the earlier investigations is that the ratio of Larmor radius to the mirror length is very high and this could have resulted in making the motion of the electron beam through the multimirror system, more non-adiabatic in comparison with the earlier experiments. The other difference, we would like to point out, is that we had the option to inject the beam with any angle between 0° - 90° , whereas in all the earlier experiments the injection was along the axis. In most of our experiments the injection angle lay in the range 30° - 40° , when the dips were found to be most pronounced and the transmitted current plot was wide enough to record several dips. Even though the injection angle in this case was very much inside the loss

cone, the significant initial perpendicular energy could have made the recording of these interactions easier.

The results mentioned in section (3.1), about the changes, noticed in transmitted current plot with the increase in the analyzer grid voltage (Fig. 3.2), indicate that not all the dips in the transmitted current correspond to reflections of the particles from the multimirror system. One should therefore understand these interactions as those leading to a transfer of energy from parallel to perpendicular direction, thus leading to an increase in the pitch angle. However some particles may get reflected from the mirrors, for example, as is the case of the dips observed even with very low analyzer grid voltages. Apparently, if one could do an experiment with injection angles, lying just inside the corresponding loss cone angle, one could achieve better conditions for the reflection of particles.

In the dependences of the positions of the dips with the square root of beam energy and injection angle, in figs. (3.3) and (3.4) we notice that even though the behaviour of the experimental curves is in good agreement with the theoretically expected dependences, yet the experimental points are situated away from the theoretical curves. One source for such deviations could be the error in determining the pitch angle. As explained in section (2.3), since the gun is placed in the region of the first minimum of the multimirror field, the angle subtended by the gun axis with that of the system was taken to be the injection angle. However, there could be errors, because of the fact

that at low mirror ratios, the edge effects are such that the field lines may not be exactly parallel to the axis of the system. A slight increase in the injection angle θ would tilt the theoretical line downwards bringing them closer to the experimental points. Another point to be noticed in connection with the observed deviations is that the experimental observations have been carried out after the beam has travelled upto the third mirror region, a factor, which the theoretical dependences (1.37) has not taken into account. For a real comparison one should make suitable modifications in the theoretical dependences, taking into account the fact that there is a reduction in the parallel energy of the particles during their passage upto the third mirror region, as is seen from the experimental results, shown in figs. (3.7) and (3.8).

A plausible explanation for the observation of increasing number of dips in the transmitted current plot as the detector is moved away from the gun is obtained from proper understanding of the relation at eqn. (1.51). The relation $\ell \Omega = n \omega_t$ corresponds to a resonance taking place when the electron completes n cyclotron rotations during its passage through ℓ spatial periods of the magnetic field. For example, $2\Omega = \omega_t$ corresponds to the coincidence of one cyclotron rotation with the transit through two mirrors and $\Omega = 2\omega_t$ corresponds to the coincidence of two electron rotations with transit through one mirror.

The various modes and orders, which follow from the relation $\ell \Omega = n \omega_t$, at various distances from the point of

injection are illustrated in fig. (4.1). The numbers in brackets correspond to the values of ℓ and n . As we had explained in section (3.1) the range of magnetic field in which the transmitted current is non-zero has a lower and upper limit (continuous curve in fig. 3.1). In the figure 4.1 we have shown the region of magnetic field values where the transmitted current is not equal to zero and also the shaded region, corresponding to zero transmitted current in the system. From the above picture it is clear that only those modes and orders, which lie within the window, corresponding to the unshaded region, could be observed in any of the experiments.

We further note that as we increase the distance of the detector from the gun by 1, 2, 3, 4, -----mirrors, in the particular illustration shown in fig. 4.1, the number of observable dips increases as is also observed in our experiments described in section (3.4). It should also be noted here that if the window is made wider, for example by decreasing the injection angle for the same beam energy, the number of observable dips becomes more. The number of observable dips will progressively increase with the increase in distance of the detector from the gun. It should be emphasized that the above explanation is a simplified description of a complex phenomenon and does not take into account the decrease in $V_{||}$ because of the resonance and the consequent shifting of the resonance to lower values of magnetic field as the particles pass through increasing number of spatial periods.

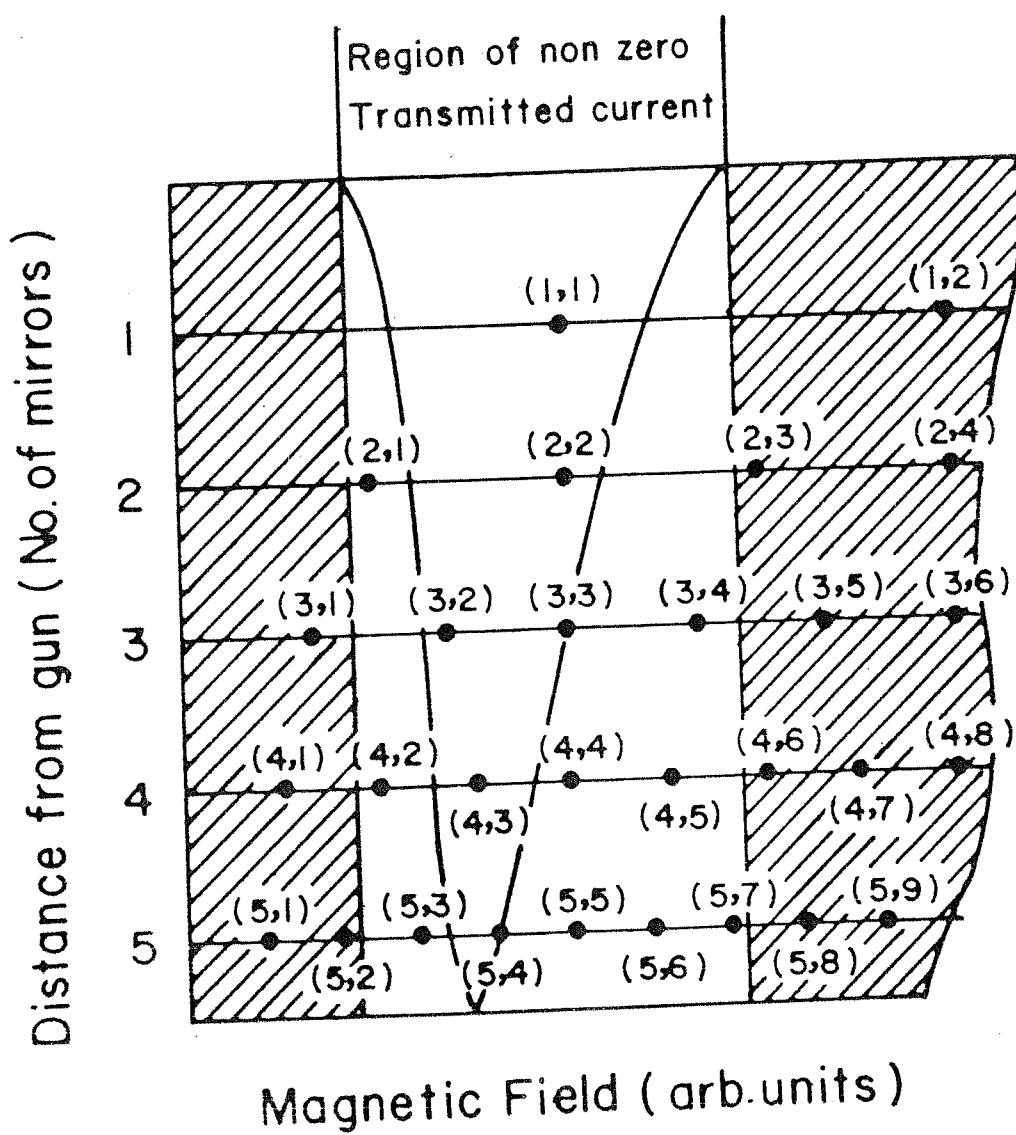


Fig. 4.1 Observable modes and orders at various distances from the electron gun.

The shifting of the dips to lower values of magnetic field described in section (3.4) could probably be explained in the light of our experimental observations mentioned in section (3.4) and also the results of Fedorchenko et al.¹⁸. The energy analysis of the transmitted electrons exhibits that the parallel energy shows a decreasing trend (fig. 3.7) with the increase in the number of mirrors travelled by the beam. A decrease in the parallel energy of the beam would in turn result in the occurrence of a resonance with a particular mode and order at a lower value of magnetic field.

Thus, as conclusions of the experimental investigations of the passage of an electron beam through a multimirror system, the main results can be summarised as under:

1. In the case of the transmission of an electron beam through a homogeneous magnetic field in the system, the transmitted electron current versus magnetic field plot exhibits monotonic rise and fall. Once the magnetic field is made spatially periodic (mirror ratio ≥ 1.03) the transmitted current is found to contain several dips, occurring at discrete values of magnetic field, at both lower and higher values than that corresponding to the relation $\Omega = \omega_t$ and in accordance with the relations $\ell \Omega = n \omega_t$ ($\ell = 1, 2, 3, 4$).
2. In order to carry out a quantitative comparison with the theoretical predictions (1.35) and (1.37) or (1.51) these experiments were repeated for different

values of initial beam energy, maintaining the other experimental parameters constant. The positions of the various dips, when plotted against the square root of initial beam energy are always found to lie on a straight line (Fig. 3.3). The different dips in the transmitted current are found to be situated close to the different theoretically predicted lines, corresponding to $2\Omega = 2\omega_t$ and $2\Omega = 3\omega_t$. The distance between the adjacent dips in the transmitted current is also found to be linearly proportional to the square root of beam energy.

3. The dependences of the positions of the first and second dips on the injection angle, plotted in fig. 3.4a, b are cosine curves, lying close to the theoretical dependences obtained for $2\Omega = 2\omega_t$ and $2\Omega = 3\omega_t$.
4. The energy spectrum of the transmitted electron beam was obtained for different values of magnetic field maintaining all other parameters constant (Fig. 3.9 and Fig. 3.10). This analysis shows that in the neighbourhood of the values of magnetic field, where the dips occur in the transmitted current plot the spectrum of parallel energy of electrons gets broadened and shifts towards lower values of energy. At the values of magnetic field, corresponding to dips, the parallel energy becomes low and at the values, where peaks appear, the spectra shift towards higher values

of energy.

5. In the experimental observations made at different distances from the electron gun we have observed that as the beam travels through more and more mirrors, the number of dips observed in the transmitted current versus magnetic field plot, increases. Further from a close observation of the plots obtained at different axial distances, it appears that as the beam travels further into the system, the dip shifts towards lower values of magnetic field.
6. A comparison of the values of the cyclotron frequency at the point of occurrence of the dips with the transit frequency for a particular case (Fig. 3.11) shows that the different dips correspond to $4\Omega = 2\omega_t$, $4\Omega = 3\omega_t$, $4\Omega = 4\omega_t$, $4\Omega = 5\omega_t$ and $4\Omega = 6\omega_t$. The above example corresponds to $\ell=4$ and $n=2, 3, 4, 5$ and 6 of the equation (1.51). There are other transmitted current versus magnetic field plots, obtained at different experimental conditions, in which the dips correspond to $\ell=1, n=1$; $\ell=2, n=2, 3$; $\ell=3, n=3, 4, 5$; $\ell=4, n=2, 3, 4, 5, 6$.
7. The observation of resonance effects for $\ell=2$ and 4 (Eq. 1.51), the dependance of the position of dips on the initial beam energy and injection angle corresponds to the "quantum conditions" $2q\Omega = n\omega_t$ for $q=1, 2$ in so far as the interaction leads to an increase of perpendicular energy at the expense of

parallel energy. In order to conclusively establish the occurrence of Bragg-like reflections, further experiments may have to be conducted to register the actually reflected electrons near the electron gun, which could not be carried out due to the physical constraints in the present device explained in Chapter II.

8. The resonance interaction observed at $\ell = 3$, which is not covered either by the relation $2q\Omega = n\omega_t$, obtained for Bragg-like reflections or by the existing theories for a transit frequency resonance, may be explained in terms of the higher order resonances $\ell\Omega = n\omega_t$, which should exist, in general, for nonlinear oscillatory systems, where the ℓ th harmonic of Ω may resonate with n th harmonics of ω_t .

It may finally be remarked that while all these resonances $\ell\Omega = n\omega_t$, $\ell = 1, 2, 3, 4$, as have been observed in our experiments, do lead to the transfer of energy from the parallel motion to the perpendicular motion, not all may culminate in the reflection of particles. According to the theory leading to (1.37) only the even order resonances should lead to Bragg-like reflections when such reflections are recorded.

Scope for Future Work

While comparing the experimentally obtained dependences of the positions of the dips with square root of beam

energy and the injection angle with the theoretical predictions, we had pointed out the necessity for working out a theoretical model, describing in detail the dynamics of charged particles in a multimirror system. So far, the existing theories lead us only to the conclusion that transfer of energy from parallel to perpendicular direction would take place under resonance conditions. During the motion through a large number of mirrors the particles, initially in resonance, would eventually get out of resonance as a result of a change in the parallel velocity and hence a change in ω_{\perp} . It is necessary to identify resonance zones and estimate the rates of transfer of energy from parallel to perpendicular component in the resonance region. From a first glance, it appears that the analytical solutions for the equations of motion of an ensemble of charged particles with a distribution in the initial conditions, may be extremely complicated.

The numerical simulations carried out by Laing and Robson²¹ and T. Mieno et al²⁴ have given important results. But these simulations are oversimplified due to the fact that the motion of a single particle is studied with definite initial conditions and hence many important questions remain unanswered. One could therefore carry out numerical simulations with a large number of particles, with a given distribution in the initial μ , in the initial phase angle etc. and study the interaction of the ensemble of particles with the multimirror system.

As far as the experimental studies are concerned it

would be necessary to carry out experiments to register the reflected electrons in the region behind the position of electron gun and further analysis to check the occurrence of Bragg-like reflections. Another interesting aspect which needs further study is the complementary phenomenon whereby electrons gain parallel energy at the expense of the perpendicular energy. Such electrons have been observed by us during the course of our experiments and have been found to exhibit peaks at certain discrete values of the magnetic fields. One would like to analyze the behaviour of these electrons to see what relations if any these transmission peaks satisfy.

References

1. T.G. Northrop, Adiabatic motion of charged particles (Interscience, New York, 1963).
2. R.K. Varma, Plasma equilibrium in magnetic confinement devices and stability of mirror machine plasmas, IAEA, Vienna, IAEA-SMR-61/105 (1981).
3. F.F. Chen, Introduction to Plasma Physics (Plenum Press, 1974).
4. V.G. Ponomarenko et al., Sov. Phys. JETP 28 1 (1969).
5. A.N. Dubinina et al., Plasma Phys. 11 551 (1969).
6. B.V. Chirikov, Plasma Phys. Accelerators, Thermonucl. Research (GB) 1 253 (1960).
7. I.B. Bernstein et al., Phys. Fluids 19 1546 (1976).
8. R.K. Varma, Phys. Rev. Lett. 26 417 (1971).
9. R.K. Varma, Phys. Rev. A31 3951 (1985).
10. D. Bora et al., Spring College on Fusion Energy, Trieste, 233 (1981).
11. B.G. Logen et al. Phys. Rev. Lett. 29 1435 (1972).
12. G.E. Budker et al. Sov. Phys. JETP 17 81 (1973).
13. A. Komori et al. Phys. Lett. 78A 143 (1980).

14. N. Sato, Int. Conf. on Plasma Physics, Nagoya, 2 138 (1980).
15. R.A. Mahaffey et al., Phys. Fluids 20 489 (1977).
16. R. Hatakeyama et al., J. Phys. Soc. Jpn. 48 707 (1980).
17. V.I. Granatstein et al. Plasma Phys. 17 23 (1975).
18. V.D. Fedorchenko et al., Sov. Phys. Tech. Phys. 4 1112 (1959).
19. K.D. Sinel'nikov et al., Sov. Phys. Tech. Phys. 5 229 (1960).
20. K.D. Sinel'nikov et al., Sov. Phys. Tech. Phys. 5 236 (1960).
21. E.W. Laing et al., Plasma Phys. (J. Nucl. Energy) 3 146 (1961).
22. R.C. Wingerson, Phys. Rev. Lett. 6 446 (1961).
23. R.A. Demirkhanov et al., Sov. Phys. Tech. Phys. 9 45 (1964).
24. T. Mieno et al., J. Phys. Jpn. 56 4347 (1987).
25. L.I. Rudakov et al., Plasma Physics & Problems of Controlled Thermonuclear Reactors, Moscow, Vol. III, 181 (Pergamon Press, 1960).

26. K.S. Golovanivsky et al., Plasma Phys. 19 1 (1977).
27. N. Minorsky, Nonlinear Oscillations, 460 (D. Van Nostrand Comp. Inc., 1962).